

Eberswalde University for Sustainable Development – HNEE
University of Applied Sciences
Faculty of Forest and Environment

Warsaw University of Life Sciences WULS – SGGW
in Warsaw
Faculty of Forestry

Gulam Mohiuddin
Album number HNEE: 19212758
Album number SGGW: 201596

Land surface temperature dynamics in a changing landscape: A time series analysis of land surface temperature data in Google Earth Engine

Dynamik der Landoberflächentemperatur in einer sich verändernden Landschaft: Eine Zeitreihenanalyse von Daten zur Landoberflächentemperatur in Google Earth Engine

Master's Thesis
on the course of – Forest Information Technology

Thesis written under the supervision of
Prof. Dr. Jan-Peter Mund
Research Professorship for Remote Sensing and GIS
HNE Eberswalde

Dr. Evelyn Wallor
FIT Coordination & Lectures
HNE Eberswalde

Eberswalde, 2023

Oświadczenie promotora pracy

Oświadczam, że niniejsza praca została przygotowana pod moim kierunkiem i stwierdzam, że spełnia warunki do przedstawienia tej pracy w postępowaniu o nadanie tytułu zawodowego.

Declaration of the promoter

I declare that this thesis was prepared under my supervision, and I state that it meets the conditions for presenting such a body of work in the process of obtaining a professional title.

Erklärung des/der Betreuers/-in

Hiermit erkläre ich, dass die vorliegende Arbeit angefertigt wurde, wurde unter meiner Leitung erstellt wurde und ich bestätige, dass sie die Bedingungen zur Verleihung des Abschluss-diploms erfüllt.

Data
Date
Datum

Podpis promotora pracy
Signature of the promoter
Unterschrift des/der Betreuers/-in

Oświadczenie autora pracy

Świadom odpowiedzialności prawnej, w tym odpowiedzialności karnej za złożenie fałszywego oświadczenia, oświadczam, że niniejsza praca dyplomowa została napisana przeze mnie samodzielnie i nie zawiera treści uzyskanych w sposób niezgodny z obowiązującymi przepisami prawa, w szczególności ustawą z dnia 4 lutego 1994 r. o prawie autorskim i prawach pokrewnych (Dz. U. Nr 90 poz. 631 z późn. zm.).

Oświadczam, że przedstawiona praca nie była wcześniej podstawą żadnej procedury związanej z nadaniem dyplому lub uzyskaniem tytułu zawodowego.

Oświadczam, że niniejsza wersja pracy jest identyczna z załączoną wersją elektroniczną. Przyjmuję do wiadomości, że praca dyplomowa poddana zostanie procedurze antyplagiatowej.

Declaration of the author

Aware of the legal liability, including criminal liability for submitting a false statement, I declare that this thesis is written by me alone and does not contain content obtained in a manner breaking applicable laws, in particular, the Act of February 4, 1994, on copyright and related rights (Journal of Laws, no. 90, item 631, as amended).

I certify that the work has not previously been the basis for any procedure in connection with obtaining a diploma or professional title.

I declare that this version of the work is identical to the attached electronic version.

I acknowledge that the thesis is subject to anti-plagiarism procedures.

Erklärung des Autors

Gesetzlicher Haftpflicht, besonders strafrechtlicher Verantwortlichkeit für Abgabe einer falschen Erklärung bewusst, erkläre ich hiermit, dass vorliegende Diplomarbeit selbständig angefertigt wurde und keinen Inhalt enthält, der widerrechtlich erworben wurde, insbesondere nicht mit dem Gesetz über Urheberrecht vom 4. Februar 1994 (GB. Nr. 90, Pos. 631 mit späteren Änderungen) übereinstimmend.

Ich erkläre auch, dass die Arbeit bisher keiner anderen Prüfungsbehörde vorgelegt wurde.

Der Durchführung einer elektronischen Plagiatsprüfung stimme ich hiermit zu. Die eingereichte elektronische Fassung der Arbeit entspricht der eingereichten schriftlichen Fassung exakt.

Data	(czytelny podpis autora).....
Date	(Signature of the author)
Datum	(Unterschrift des Autors der Arbeit)

Streszczenie

To jest badanie, które bada przestrzenno-czasowe wzorce temperatury powierzchni lądowej (LST) i jej związek ze zmianami w użytkowaniu ziemi / pokryciem ziemi (LULC) w miejskim otoczeniu. Główne cele to analiza zmienności sezonowej, trendów LST i reakcji LST na różne typy LULC w zidentyfikowanych punktach krytycznych, w tym korelacji między nimi. Zastosowano podejście mieszane, wykorzystując techniki teledetekcyjne i dane o temperaturze powierzchni lądu Landsat do zbierania danych regionalnych. Próbka obejmowała 462 obrazy dzielnicy Chbar Ampov (Phnom Penh, Kambodża) wykonane od 2000 do 2021 roku, które zostały przeanalizowane przy użyciu platformy opartej na chmurze Google Earth Engine (GEE). Wyniki wykazały zauważalną zmienność sezonową w LST i wizualne powiązanie między LST a zmianami LULC w konkretnych hotspots. Nie zaobserwowano długoterminowych trendów w LST, mimo wahania do 49 °C. Zidentyfikowano silną dodatnią korelację między obszarami zabudowanymi a LST, podczas gdy negatywne korelacje stwierdzono między LST a ciałami wodnymi i roślinnością. Wyniki te popierają koncepcję, że urbanizacja, uszczelnianie ziemi i zmiany LULC są ściśle związane z wahaniem LST, podkreślając wagę uwzględnienia lokalnego kontekstu i konkretnych zmian LULC podczas badania dynamiki LST. Wyniki te mogą informować strategie planowania i zarządzania miejskiego, takie jak włączanie zielonej i niebieskiej infrastruktury, aby umiarkować wartości LST i poprawić środowisko miejskie. To badanie dostarcza cennych informacji o dynamice LST i związku między LST a zmianami LULC, z potencjalnymi implikacjami dla urbanistów, decydentów i badaczy pracujących nad stworzeniem bardziej zrównoważonych i odpornych środowisk miejskich.

Słowa kluczowe: temperatura powierzchni ziemi (LST), dynamika termiczna, wzorce przestrzenno-czasowe, zrównoważone planowanie miejskie, użytkowanie ziemi i pokrycie ziemi (LULC)

Abstract

This study investigates the spatiotemporal patterns of land surface temperature (LST) and its relationship with land use/land cover (LULC) changes in an urban setting. The main objectives were to analyse seasonal variability, LST trends, and the response of LST to different LULC types in identified hotspots, including the correlation between them. A mixed-methods approach was employed, utilising remote sensing techniques and Landsat Land surface temperature data to collect regional data. The sample included 462 images of the Chbar Ampov District (Phnom Penh, Cambodia) taken from 2000 to 2021, which were analysed using the cloud-based platform Google Earth Engine (GEE). The findings revealed noticeable seasonal variability in LST and a visual connection between LST and LULC changes in specific hotspots. No long-term trends in LST were observed, despite fluctuations up to 49 °C. A strong positive correlation between built-up areas and LST was identified, while negative correlations were found between LST and water bodies and vegetation. These results support the notion that urbanisation, land sealing and LULC changes are closely related to LST variations, emphasising the importance of considering local context and specific LULC changes when examining LST dynamics. The findings can inform urban planning and management strategies, such as incorporating green and blue infrastructure to moderate LST values and improve the urban environment. This study provides valuable insights into LST dynamics and the relationship between LST and LULC changes, with potential implications for urban planners, policymakers, and researchers working towards creating more sustainable and resilient urban environments.

Keywords: Land surface temperature (LST), Thermal dynamics, Spatiotemporal patterns, Sustainable urban planning, Land use land cover (LULC)

Zusammenfassung

Diese Studie untersucht die raumzeitlichen Muster der Landoberflächentemperatur (LST) und ihre Beziehung zu Veränderungen der Landnutzung und Landbedeckung (LULC) in einer städtischen Agglomeration. Die Hauptziele bestehen darin, die saisonale Variabilität, LST-Trends und die Reaktion der LST auf verschiedene LULC-Typen in identifizierten Hotspots, einschließlich der Korrelation zwischen ihnen, zu analysieren. Es wird ein Mixed-Methods-Ansatz verwendet, der Fernerkundungstechniken und Landoberflächentemperatur Daten Landsat-Bilder zur Analyse nutzt. Die Stichprobe umfasst 462 Bilder des Chbar Ampov Distrikt, Phnom Penh, Kambodscha, die zwischen 2000 und 2021 aufgenommen und mit der cloudbasierten Plattform Google Earth Engine (GEE) analysiert wurden. Die Ergebnisse zeigen eine signifikante saisonale Variabilität der LST und eine visuelle Verbindung zwischen LST- und LULC-Veränderungen in bestimmten Hotspots. Es werden keine langfristigen Trends in der LST beobachtet, jedoch Schwankungen bis zu 49°C. Eine starke positive Korrelation wurde zwischen bebauten Flächen und LST festgestellt, während negative Korrelationen zwischen LST und Gewässern sowie Vegetation nachgewiesen wurden. Diese Ergebnisse unterstützen die Hypothese, dass Variationen in der Bodenoberflächentemperatur (LST) eng mit Faktoren wie Urbanisierung, Bodenversiegelung und Veränderungen in der Landnutzung und -bedeckung (LULC) verbunden sind. Das verdeutlicht die Notwendigkeit, bei einer Analyse von Veränderungen in der LST, die lokalen Besonderheiten und spezifischen Veränderungen in LULC zu berücksichtigen. Die Ergebnisse können städtische Planungs- und Managementstrategien unterstützen, wie zum Beispiel die Integration von grüner und blauer Infrastruktur, um LST-Werte zu modifizieren und die bekannte Städtische Hitzeinsel zu reduzieren. Diese Studie bietet wertvolle Einblicke in die LST-Dynamik und die Beziehung zwischen LST- und LULC-Veränderungen, mit möglichen Implikationen für Stadtplaner, politische Entscheidungsträger und Forscher, die an der Schaffung nachhaltigerer und widerstandsfähigerer städtischer Umgebungen arbeiten.

Schlüsselwörter: Bodenoberflächentemperatur (LST), thermische Dynamik, raumzeitliche Muster, nachhaltige Stadtplanung, Bodennutzung und Bodenbedeckung (LULC)

Zgadzam się udostępnić moją pracę w czytelniach biblioteki SGGW, w tym w Archiwum Prac Dyplomowych SGGW.

I consent to making my work accessible in the reading rooms of the SGGW library, including the SGGW Theses Archive.

Ich stimme zu, meine Arbeit in den Lesesälen der SGGW-Bibliothek, einschließlich des SGGW-Theses-Archivs, zugänglich zu machen.

.....

(czytelny podpis autora)
(legible signature of the author)
(lesbare Unterschrift des Autors der Arbeit)

Contents

List of figures	II
List of tables	III
List of abbreviations	III
List of equations	IV
Working definitions	IV
1 Introduction	1
1.1 A brief overview of LST and UHI	1
1.2 LST analysis with different satellite thermal scanners	3
1.3 Research aim and objectives	5
2 Material and Methods	5
2.1 Remote sensing data	5
2.2 Software and platforms used for the analysis	6
2.3 Study area	7
2.4 Methods	8
2.4.1 Processing of Landsat data	9
2.4.2 LST ranges, seasonal variation, and trend analysis	13
2.4.3 LST vs LULC relationship analysis	15
3 Results	17
3.1 Overview of LST distribution and ranges during 2000 - 2021	17
3.2 Seasonal variability of LST	21
3.3 Trend of LST and hotspots identification	23
3.4 Response of LST to different LULC in identified hotspots	26
3.5 Correlation between LST and different land covers	29
4 Discussion	32
4.1 Overview of the study objectives and the key findings	32
4.2 Discussion on data and methods	32
4.3 Discussion on results	34
4.4 Theoretical and practical implications of the study findings	35
4.5 Limitations of the study	36
4.6 Future research directions	37
5 Conclusion	38
References	39

List of figures

Figure 1: Cloud coverage in the Landsat images selected for the study	6
Figure 2: Sensor-wise number of Landsat images for the period of 2000 to 2021 (60% maximum cloud filter applied).....	6
Figure 3: Location of the study area.....	7
Figure 4: Graphical overview of simplified methodical workflow	8
Figure 5: LST estimation and spectral indices calculation from Landsat images.....	9
Figure 6: Location of random points for correlation test	16
Figure 7: Boxplot of minimum, mean & maximum LST	18
Figure 8: Calendar heatmaps of LST. a. mean, b. maximum & c. minimum	19
Figure 9: Annual LST range.....	20
Figure 10: Number of warmer months per year in LST categories	21
Figure 11: Spatial-seasonal variation in LST	22
Figure 12: Monthly minimum, mean and maximal LST in 2015	22
Figure 13: Example of unusual monthly fluctuation in LST	23
Figure 14: Total time series of minimum, mean & maximum LST (2000 - 2021).....	24
Figure 15: Time series with error bands chart of LST	24
Figure 16: LST in 2000 - 2021	25
Figure 17: Location of identified 5 hotspots (background map is from April 2015).....	26
Figure 18: LST and LULC changes in point 1	27
Figure 19: LST and LULC changes in point 2.....	28
Figure 20: LST and LULC changes in point 3	29
Figure 21: Correlation matrix between LST, IBI, MNDWI & NDVI	30
Figure 22: Linear relationship between built-up area and LST	30
Figure 23: Relationship between water and LST;	31
Figure 24: Relationship between vegetation and LST;	31
Figure 25: Revised correlation matrix between LST, IBI, MNDWI & NDVI	32

List of tables

Table 1: Renaming of the bands from different sensors (cf. column “New name”)	9
Table 2: Example of extracted data from processed Landsat images	13
Table 3: Scale for the identifying comparatively warmer months	14
Table 4: Example of the extracted data for visual LST vs LULC relationship analysis	15
Table 5: Example of the extracted data for correlation test	16
Table 6: Descriptive statistics of minimum, mean & maximum LST	17

List of abbreviations

BT = Brightness temperature

CFMask = C-Function-of-Mask

GEE = Google Earth Engine

IBI = Indices-based built-up index

LST = Land surface temperature

LULC = Land use land cover

MODIS = Moderate Resolution Imaging Spectroradiometer

MNDWI = Modified Normalised Difference Water Index

NDBI = Normalised Difference Built-up Index

NDVI = Normalised Difference Vegetation Index

NDWI = Normalised Difference Water Index

NIR = Near infrared

PV = Proportion of vegetation

SLSTR = Sea and Land Surface Temperature Radiometer

SR = Surface reflectance

SWIR = Shortwave infrared

TC = Tasseled cap

TIR = Thermal infrared

TOA = Top-of-atmosphere

UHI = Urban heat island

List of equations

Equation 1: Equation for calculating radiance	10
Equation 2: Equation for calculating brightness temperature	10
Equation 3: Equation for calculating MNDWI	10
Equation 4: Equation for calculating IBI	11
Equation 5: Equation for calculating NDVI.....	11
Equation 6: Equation for calculating proportion of vegetation.....	11
Equation 7: Equation for calculating emissivity	11
Equation 8: Calculating Tasseled cap components	12
Equation 9: Equation for estimating LST	12
Equation 10: Equation for calculating Gamma (γ).....	12
Equation 11: Equation for calculating Delta (δ)	12
Equation 12: Equation for atmospheric functions.....	13

Working definitions

Thermal dynamics:

In this study thermal dynamics is expressed by land surface temperature (LST) and it is often used synonymously addressing each other.

Temperature:

In this study, temperature always means LST unless it is specifically mentioned otherwise.

Basic land covers:

Basic land covers include water, vegetation, and built-up areas, represented by respective spectral indices MNDWI, NDVI and IBI. Hence, in this study, when remarks about these land covers are made, it is always based on values from these indices.

Three categories of LST:

Another frequently used term in this study is three categories of LST. Three categories of LST always imply minimum, mean and maximum LST in this study unless said specifically something else.

Hotspots:

In this study, hotspot simply means the areas that are frequently appearing as warmer spots in the visual interpretation.

1 Introduction

This section provides a comprehensive background and rationale for this study, focusing on the impact and implications of Land Surface Temperature (LST) and the Urban Heat Island (UHI) effect. Beginning with a detailed overview of LST and its relationship to urbanisation and UHI, it explores the multitude of effects UHI has on urban environments, including health implications, ecosystem disruptions, energy consumption, and local climate changes. The subsequent discussion underscores the importance of understanding these effects to enable policymakers and urban planners to devise effective mitigation strategies. The analysis then delves into the time series analysis of LST data as a potent tool to reveal spatiotemporal patterns of urban LST. Further in the discussion, the role of remote sensing data is explored, noting the benefits of different data sources. Finally, the chapter concludes by examining the relationship between LST and Land Use and Land Cover (LULC) types and the use of spectral indices in understanding this relationship. The discussion sets the stage for a deeper investigation into the dynamics of LST and UHI and their implications for urban planning and environmental management.

1.1 A brief overview of LST and UHI

LST is a crucial parameter in understanding the surface energy balance and the heat exchange between the Earth's surface and the atmosphere (Weng, 2009). In simple terms, LST is the skin temperature of the surface. With rapid urbanisation, the built environment contributes to a steep increase in LST, contributing to the urban heat island (UHI) effect. UHI is a phenomenon where human activities and alterations in land use lead to higher temperatures in cities compared to neighbouring rural areas (Oke et al., 1987). Time series analysis of LST data has emerged as a practical approach to understanding the spatiotemporal patterns of urban LST, providing vital insights for effective urban planning and environmental management.

Understanding the UHI effect is crucial to urban planners and decision-makers because UHI has a multitude of negative impacts on the urban environment. One of the most critical consequences of UHI is its impact on public health. High temperatures in urban areas can exacerbate heat-related illnesses (Kovats & Hajat, 2008). Furthermore, vulnerable populations, including the elderly, children, and low-income communities, are particularly susceptible to heat-related health risks (Hondula et al., 2014). UHI can also influence the distribution of vector-borne diseases by providing suitable habitats for

disease-carrying organisms (Patz et al., 2005). UHI contributes to increased energy consumption, particularly for air conditioning in different buildings (Santamouris, 2014a).

UHI can influence local climate by altering atmospheric circulation patterns, leading to changes in precipitation, cloud cover, and wind patterns (Zhang et al., 2010). These local climate changes can, in turn, exacerbate UHI effects, creating a positive feedback loop that further increases urban temperatures (Meehl & Tebaldi, 2004). Higher temperatures in urban areas due to UHI can also form ground-level ozone and other air pollutants (Jacob & Winner, 2009). UHI can also impact urban ecosystems, altering species distribution, behaviour, and interactions (Grimm et al., 2008). The increased temperatures can affect plant phenology, species composition, and ecosystem productivity (Pickett et al., 2004).

Understanding these effects of UHI is essential for policymakers and urban planners to develop and implement effective mitigation strategies, such as increasing green spaces, promoting energy-efficient buildings, and employing cooler surface technologies (Akbari et al., 2001). By addressing UHI's challenges, urban areas can achieve more sustainable, healthy, and resilient communities. Understanding the thermal dynamics of an area can provide insight into understanding these UHI-related effects.

Time series analysis of LST data provides a robust method for understanding the spatiotemporal patterns of urban LST and, thus, the thermal dynamics (Nagler et al., 2013). Time series analysis involves examining LST data collected at regular intervals over an extended period, which can reveal trends, seasonality, and fluctuations in LST (Box et al., 2015). Time series analysis of LST data offers valuable insights for urban planning and environmental management, as it can identify areas with consistently high LST (hotspot), detect changes in LST due to land use change, and evaluate the effectiveness of mitigation measures against the effects of UHI (Nagler et al., 2013).

Time series analysis of LST in an urban area includes several key benefits. Firstly, time series analysis of LST can help pinpoint areas that consistently exhibit high LST, indicating the presence of so-called hotspots. Such information can assist urban planners in prioritising interventions for reducing LST (Erell et al., 2012). Secondly, time series analysis of LST can detect changes in LST due to land use change, such as urban expansion or reforestation efforts (Weng, 2009). Thirdly, such time series analysis can assess the effectiveness of LST reduction strategies, such as increasing green spaces, implementing cool roofs, or adopting low-impact development practices

(Santamouris, 2014b). By comparing LST data before and after implementing these measures, urban planners can determine their efficacy and optimise resource allocation for future interventions (Kleerekoper et al., 2012). In addition, time series analysis of LST data can inform the development of climate-resilient urban design by providing insights into how LST patterns change over time and under different climatic conditions. This information can help design urban spaces better adapted to local climate patterns and mitigate the UHI effect (Erell et al., 2012). Time series analysis of LST data can also support public health interventions by identifying areas with increased heat-related health risks. Public health agencies can use this information to target vulnerable populations and develop early warning systems for heatwaves, reducing heat-related morbidity and mortality (Hajat et al., 2010).

1.2 LST analysis with different satellite thermal scanners

The use of remote sensing has notably improved the availability and accuracy of LST data, enabling researchers to monitor urban LST at various spatial and temporal resolutions (Weng et al., 2004; Wan et al., 2004). Several open-source remote sensing data types are helpful for LST time series analysis, including Landsat, Moderate Resolution Imaging Spectroradiometer (MODIS), and Sentinel-3. The different data sources have different benefits in terms of spatial resolution, study area size, study period and frequency of data. MODIS data provides daily global coverage and can be used to track the temporal variation of LST. However, the spatial resolution of thermal infrared data from MODIS is around 1 km (Wan, 2008). Sentinel-3, like many other European Space Agency satellites, carries a thermal infrared sensor called the Sea and Land Surface Temperature Radiometer (SLSTR). The SLSTR sensor measures the temperature of the land and sea surface, providing LST data with a high spatial resolution of around 500 m (Coppo et al., 2013). Landsat thermal data can be a good option considering its temporal coverage, spatial resolution and consistency (Weng, 2009). Landsat has been collecting data since 1972, which provides a long-term time series of LST data in urban areas. Hence Landsat data allows for examining temporal patterns and trends in LST over several decades, providing valuable insight into how urban heat islands (UHIs) develop and change over time. The thermal infrared data from Landsat has a spatial resolution of around 100 m, sufficient to capture variations in LST in urban areas, allowing for identifying specific hot spots within urban areas and can help inform targeted mitigation strategies. Landsat data is collected with consistent

methods and sensor settings, which ensures that the time series has consistency, which is essential for conducting a time series analysis (Mildrexler et al., 2011).

The UHI effect arises from reduced vegetation cover, increased impervious surfaces, and high energy consumption (Arnfield, 2003). These factors alter the surface energy balance, leading to an increase in LST. In urban environments, impervious surfaces such as concrete and asphalt have a higher heat capacity and thermal conductivity than natural surfaces, causing them to absorb and store more solar energy (Asimakopoulos, 2001).

Several studies have investigated the connection between LST and LULC. In a study by Weng et al. (2008), the authors utilised satellite imagery and remote sensing data to analyse the spatial distribution of LST in various LULC types. Their results indicate that highly urbanised areas with impervious surfaces and reduced vegetation cover experienced elevated LSTs. Similarly, Amiri et al. (2009) investigated the impact of different LULC types on LST using Landsat satellite data. Their findings revealed that high-density urban areas with a predominance of concrete and asphalt surfaces exhibit higher LST values than low-density residential areas with more green spaces.

The relationship between LST and different LULC types is often analysed using the LST and value from different spectral indices representative of different land covers. Rouse et al. (1973) proposed the NDVI to quantify vegetation density and health based on the difference in reflectance between the visible red and near-infrared (NIR) portions of the electromagnetic spectrum. NDVI is a widely used spectral index to study the relationship between LST and vegetation (Carlson et al., 1994; Moran et al., 1997; Gillies et al., 1997; Sandholt et al., 2002). Sobrino et al. (2001) analysed the relationship between LST and vegetation indices, such as the Normalised Difference Vegetation Index (NDVI). Their study confirmed that areas with higher NDVI values, indicative of denser vegetation cover, exhibited lower LSTs.

Zha et al. (2003) introduced the normalised difference built-up index (NDBI) for identifying built-up areas, which is arguably the most widely used index representing built-up areas. Since then, NDBI has been adopted in many recent studies (Xu, 2008; He et al., 2010; Kumar et al., 2012; Zhou et al., 2014; & Bouhennache et al., 2019). However, this straight forward simple index has some limitations in accurately identifying the built-up areas (Mohamed & Worku, 2019; Li et al., 2018; Nguyen et al., 2018; Dutta et al., 2015; Rahman et al., 2012; Maktav & Erbek, 2005). Indices-based built-up index (IBI) addresses the difficulty distinguishing between built-up and non-

built-up areas using thematic bands (Xu, 2008). Instead of just comparing bands, IBI uses three land use indices that cover the essential components of the urban ecosystem - vegetation, water, and built-up area.

Normalised difference water index (NDWI) extracts waterbodies using a spectral index using green and near-infrared bands (NIR) (McFeeters, 1996). Later, it was argued that typical NDWI includes noise from the built-up area, and Xu (2006) proposed a modified version of the index to address this challenge. This modified version of NDWI uses a middle-infrared band (e.g. band 6 in Landsat 8) instead of NIR, and Xu (2006) termed it the modified normalised water index (MNDWI).

1.3 Research aim and objectives

Against this backdrop, this study aims to conduct a time series analysis of LST using Landsat data to understand the thermal dynamics in Chbar Ampov district, Phnom Penh, Cambodia, from 2000 to 2021. The specific objectives are:

1. To obtain an overview of LST distribution and ranges during 2000 - 2021
2. To observe the seasonal variation and trend of LST and identify possible hotspots
3. To examine the identified hotspots and observe how LST responds in different LULC
4. To examine the relationship between LST and LULC classes (vegetation, water and built-up areas)

2 Material and Methods

This section presents an in-depth description of the material and methods used for this study. The narration starts with a short description of the primarily used remote sensing data (Landsat images). Google Earth Engine's (GEE) utility as an open-source, cloud-based platform that can manage large datasets, and automate data processing, is underlined. The geographical focus of this study, Chbar Ampov District in Phnom Penh, Cambodia, is also introduced, detailing its geographical characteristics, climate, population, and infrastructural developments. A detailed overview of the methodological workflow and steps concludes this section.

2.1 Remote sensing data

The study primarily used the Landsat data for LST estimation and calculating different spectral indices. This study used collection-1: Tier 1 data from Landsat 5, 7 and 8. Both surface reflectance (SR) and calibrated top-of-atmosphere (TOA) data were used. The

images in Phnom Penh is highly susceptible to the presence of cloud. Hence, a maximum of 60% cloud filter is applied. The cloud coverage of the selected images is presented in the following chart (Figure 1). Each dot represents an image that was considered for this study. After applying the cloud filter, 462 images were found from 2000 to 2021 (Figure 2).

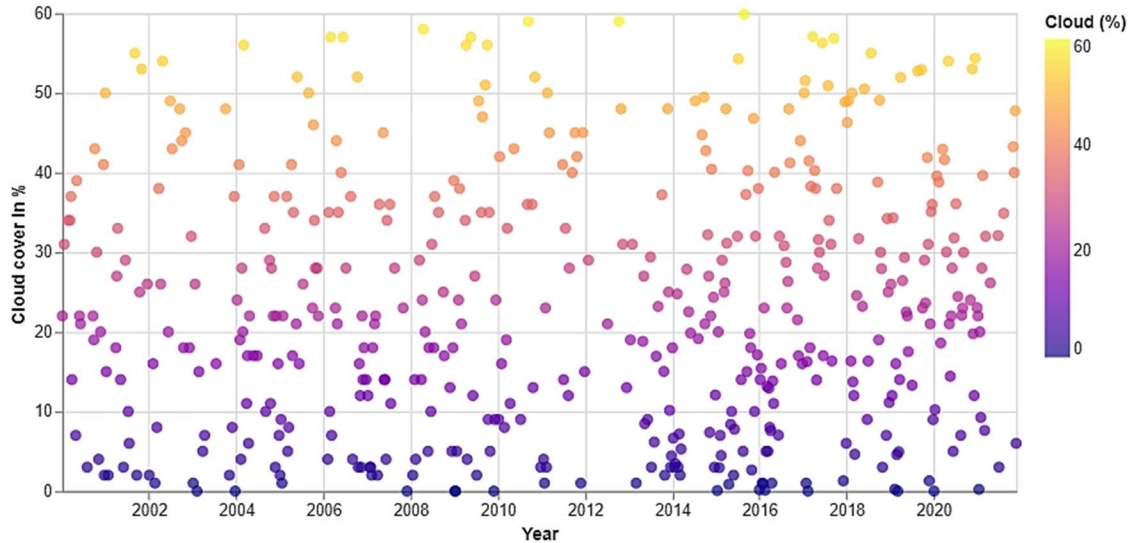


Figure 1: Cloud coverage in the Landsat images selected for the study

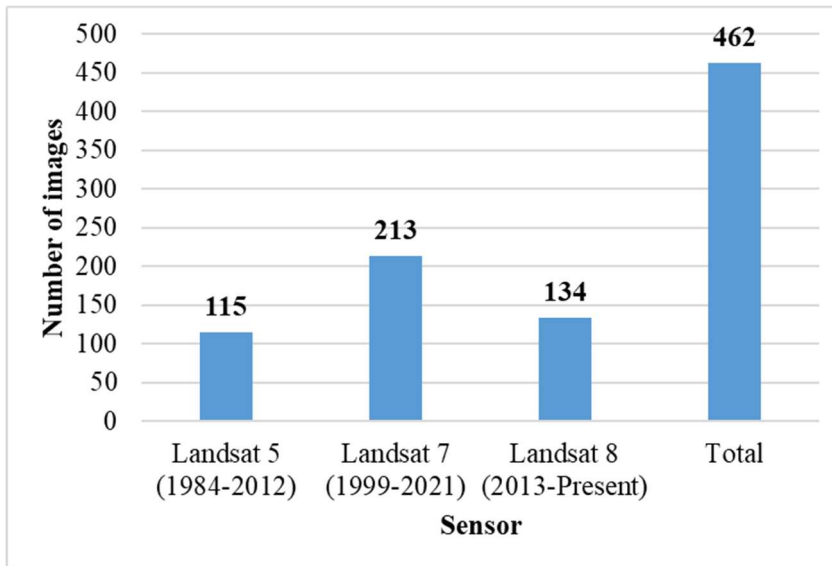


Figure 2: Sensor-wise number of Landsat images for the period of 2000 to 2021 (60% maximum cloud filter applied)

Apart from the Landsat images, images from Google Earth are used to visually compare the LST and LULC changes in the identified hotspots.

2.2 Software and platforms used for the analysis

The study used GEE (<https://earthengine.google.com/>) to access Landsat data archives to process the Landsat images to estimate LST and extract necessary statistical data.

Since GEE is a cloud-based platform, the data processing was carried out using the GEE server's computational power rather than relying on the resources of a local computer. Google Colaboratory, also known as Google Colab, was used as the platform for the analysis where it is possible to call the GEE server to access the required data. Python is used to process the images, extract datasets and for statistical analyses. Google Earth was used to extract images to compare with LST and LULC changes. ArcGIS was used to produce map layouts.

2.3 Study area

Chbar Ampov District, located in the southeast region of Phnom Penh, Cambodia, is a rapidly developing urban area with a mix of residential and commercial zones (City of Phnom Penh, 2020). The Mekong River borders the district to the east, Meanchey District to the west, Kandal Province to the north, and Prek Pnov District to the south (Figure 3).

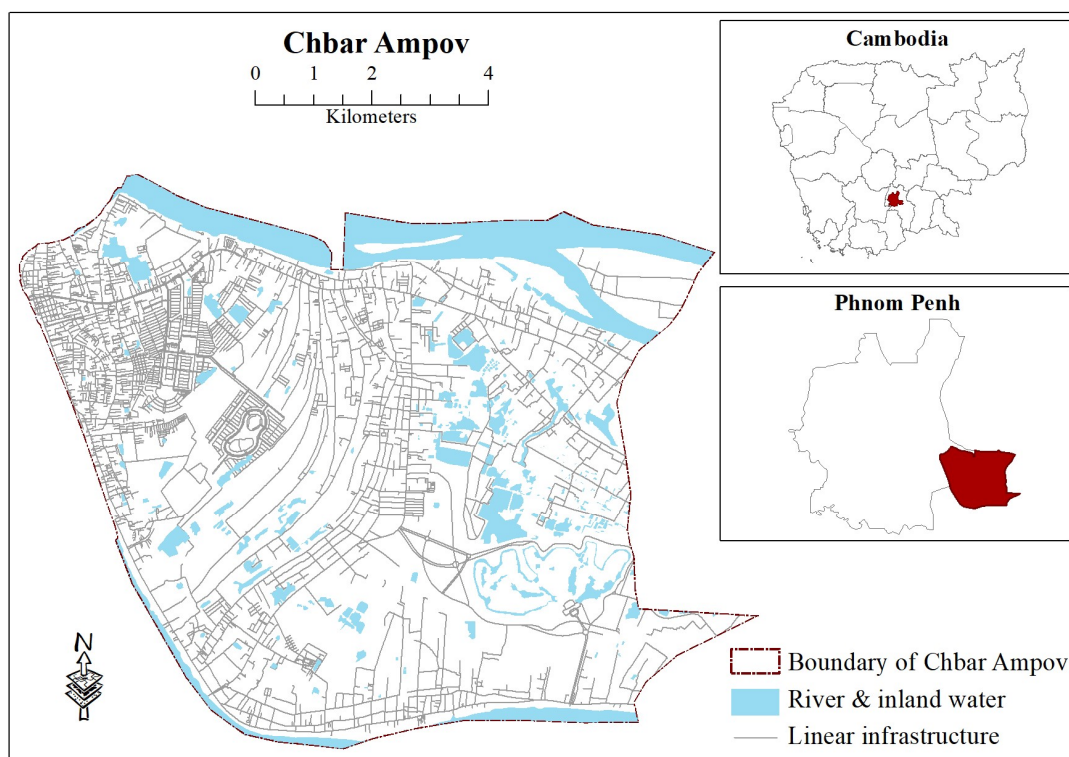


Figure 3: Location of the study area

Spanning approximately 62.52 square km, Chbar Ampov is home to an estimated population of 210,000 people (National Institute of Statistics, 2020). The district enjoys a tropical wet and dry climate, characterised by distinct wet (May to October) and dry (November to April) seasons, with an average annual temperature of around 27.5 degrees Celsius (Meteorological Department of Cambodia, 2021). Chbar Ampov's physiography consists of mostly lowland plains, which makes it susceptible to seasonal

flooding due to its proximity to the Mekong River (Mekong River Commission, 2021). Notable features of Chbar Ampov include its numerous pagodas and cultural sites, as well as its bustling markets and thriving local businesses. The district continues to develop rapidly, with new infrastructures and residential projects reshaping its landscape and contributing to its growing importance within Phnom Penh (City of Phnom Penh, 2020).

2.4 Methods

The methods of this study are expressed through three different distinctive parts (Figure 4). Firstly, processing of Landsat data to estimate LST and spectral indices, including extracting statistical data from the processed images.

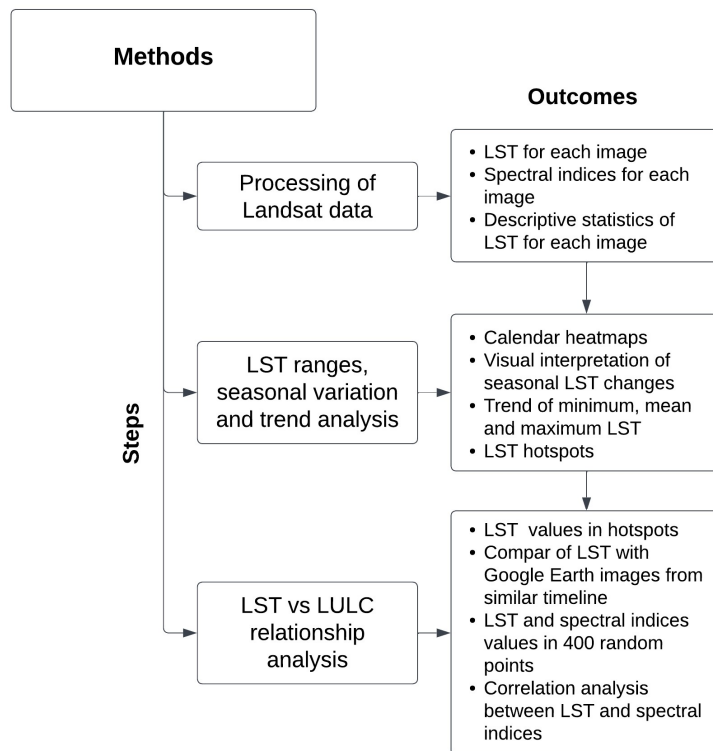


Figure 4: Graphical overview of simplified methodical workflow

The results of the processed LST are used in the second part for visual interpretations (seasonal variation and visual trend), which leads to identifying hotspots (consistently warmer spots). On the other hand, the extracted descriptive data is used for descriptive statistics and trend analysis. The third and final part includes the analysis of the relationship between LST and LULC. The LST in the identified hotspots were compared to Google Earth from a similar timeframe to understand the relationship visually. Then a correlation analysis was conducted using LST and three different spectral indices values (IBI, MNDWI, NDVI) on 400 random points to understand the relationship quantitatively.

2.4.1 Processing of Landsat data

This section comprehensively describes the processing of the Landsat data, including all necessary steps and algorithms (Figure 5). The section also includes a detailed methodological description of data extraction from the processed images, seasonal variation analysis, trend analysis and hotspot identification. The equations for estimating LST are from the study by Nill et al. (2019).

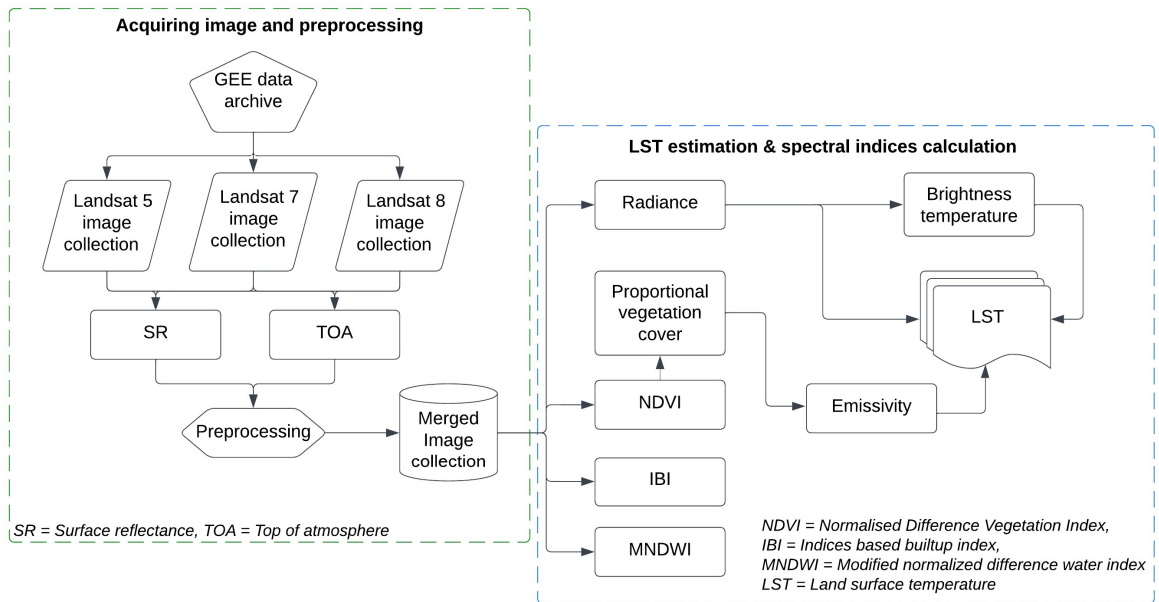


Figure 5: LST estimation and spectral indices calculation from Landsat images

A step by step is description is provided below to explain the processing of Landsat data:

a) Cloud filter and masking

The study only considered images with less than 60% cloud cover (Figure 5). A cloud mask is also applied to filter out the existing cloudy pixels using the C-Function-of-Mask (CFMask) algorithm (Foga et al., 2017).

b) Making the band names coherent

Band names were renamed to make coherent and simple use of the same algorithms for all three collections (Table 1).

Table 1: Renaming of the bands from different sensors (cf. column “New name”)

Band	Landsat 5	Landsat 7	Landsat 8	New name
Blue	B1	B1	B2	B
Green	B2	B2	B3	G
Red	B3	B3	B4	R
Near Infrared	B4	B4	B5	NIR
Short wavelength infrared	B5	B5	B6	SWIR1
Short wavelength infrared	B7	B7	B7	SWIR2
Thermal band	B6	B6	B10	TIR

c) Clipping to the area of interest

All the images were clipped to the boundary of the study area (Chbar Ampov District).

d) Radiometric calibration: Radiance

Radiometric calibrations were performed on TOA and SR products converting the raw digital values in the image data to physical units of radiance or reflectance to ensure that the data is accurately calibrated and can be used for quantitative analysis and comparison with other data sets (Chander et al., 2003). Radiance was obtained by following the equation (Equation 1):

$$L = ML \times DN + AL \quad (1)$$

Where, L is radiance, ML is band specific multiplicative factor, AL is the band specific additive factor.

e) Thermal calibration: brightness temperature (BT)

Brightness temperature (BT) is the temperature of an object that emits radiation at a specific wavelength. In Landsat, the BT measures the radiance emitted from the Earth's surface in the thermal infrared (TIR) wavelength region. The BT values are required to estimate the LST. BT was measured from the TOA product using the thermal calibration constants from the metadata of the respective image collection and based on Planck's law (Chander et al., 2009). BT was obtained by following the equation (Equation 2):

$$BT = \frac{K_2}{\ln(\frac{K_1}{L} + 1)} - 273.15 \quad (2)$$

Where, BT is brightness temperature, L is radiance and K_1 , K_2 are band specific thermal calibration constants.

f) Calculating spectral indices

Three difference spectral indices were calculated using SR products for this study, representing three major components (vegetation, water and built-up area) of the landscape dynamics of the study area. The indices are MNDWI, IBI and NDVI.

MNDWI was obtained with following equation (Equation 3):

$$MNDWI = \frac{G - SWIR1}{G + SWIR1} \quad (3)$$

Where, G is green band and SWIR1 is the short-wave infrared band.

IBI was obtained from following equation (Equation 4):

$$IBI = \frac{2SWIR1 / (SWIR1+NIR) - [NIR / (NIR+R) + G / (G+SWIR)]}{2SWIR1 / (SWIR1+NIR) + [NIR / (NIR+R) + G / (G+SWIR)]} \quad (4)$$

Where, SWIR1 is the short-wave infrared band, NIR is near infrared band, R is red band, G is green band (Table 1).

NDVI was obtained using following Equation (Equation 5):

$$NDVI = \frac{NIR - R}{NIR + R} \quad (5)$$

Where, NIR is near infrared and R is visible red band.

g) Calculating proportion of vegetation (PV)

The proportion of vegetation (PV) can help account for the effects of vegetation on the thermal radiation emitted from the land surface. Vegetation cover can affect the energy balance of the land surface, leading to lower LST values due to increased evapotranspiration and shading. By incorporating PV information into LST estimation models, LST estimation accuracy can improve, particularly in areas with high vegetation cover (Carlson & Ripley, 1997). PV was calculated using the following equation (Equation 6):

$$P_v = \left(\frac{NDVI - NDVI_{min}}{NDVI_{max} - NDVI_{min}} \right)^2 \quad (6)$$

Where, $NDVI_{max}$ and $NDVI_{min}$ were chosen as 0.86 and -0.64 respectively considering the NDVI range for the study area.

h) Calculating emissivity

Emissivity is a property of a material that describes its ability to emit thermal radiation. The emissivity of a material depends on its physical properties, such as its composition, structure, and surface roughness (Flynn et al., 2001). In this study, land surface emissivity was calculated using the Simplified NDVI Threshold Method (SNDVITHM) (Sobrino et al., 2008) by applying the following equation (Equation 7):

$$E_m = \begin{cases} E_s + (E_v \frac{E_s}{E_v} E_s) P_v & NDVI < NDVI_{min} \\ NDVI_{min} \leq NDVI \leq NDVI_{max} \\ NDVI > NDVI_{max} \end{cases} \quad (7)$$

Where, E_s is emissivity of soil or bare ground, E_v is emissivity of vegetation and P_v is the proportion of vegetation. For this study the emissivity of soil and vegetation were selected as 0.97 and 0.985 following a previous study (Li et al., 2013).

i) Calculating Tasseled cap (TC) components

Tasseled cap (TC) transformation was originally developed for Landsat data (Crist & Cicone, 1984). TC transformation generates three primary components: brightness, greenness, and wetness. The brightness component is related to the overall reflectance or radiance of the scene, while the greenness and wetness components are related to vegetation cover and soil moisture content, respectively. TC components were obtained using the following equation (Equation 8):

$$TC = B * 0.0315 + G * 0.2021 + R * 0.3102 + NIR * 0.1594 + SWIR1 * (-0.6806) + SWIR2 * (-0.6109) \quad (8)$$

Where, TC is the Tasseled Cap; B, G, R, NIR, SWIR1, and SWIR2 are the reflectance values in the blue, green, red, near-infrared, shortwave infrared 1, and shortwave infrared 2 bands, respectively; the coefficients (0.0315, 0.2021, 0.3102, 0.1594, -0.6806, -0.6109) represent the weights assigned to each band in the TC transformation taken from Nitze & Grosse (2016).

j) Estimation of LST

This study utilised a Single-Channel (SC) algorithm to obtain LST that includes the surface emissivity and atmospheric conditions (Equation 9). This approach was selected due to its simplicity when the relevant parameters are known and its accuracy for sensors equipped with a single thermal band, such as Landsat TM (thematic mapper) and ETM+ (enhanced thematic mapper) (Jiménez-Muñoz & Sobrino, 2003). The equation is based on Jiménez - Muñoz et al., 2008:

$$LST = \gamma \left[\frac{1}{E_m} (\psi_1 L) + \psi_2 + \psi_3 \right] + \delta \quad (9)$$

Where, γ is calculated by equation 10, E_m is emissivity, ψ are the atmospheric functions derived from equation 12, L is the spectral radiance in the sensor and δ is calculated by equation 11:

$$\gamma = \frac{BT^2}{b_\gamma \times L} \quad (10)$$

$$\delta = BT - \frac{BT^2}{b_\gamma} \quad (11)$$

Where BT is brightness temperature, b is a sensor specific constant which are 1256 K, 1277 K, or 1324 K for Landsat 5, 7 and 8 (Jiménez-Muñoz et al., 2014).

The atmospheric functions (Equation 12) provide information about the transmissivity, upwelling, and downwelling radiation of the atmosphere and are estimated based on the amount of atmospheric water vapour using a second-degree polynomial approximation following Lantz et al. (2010).

$$\begin{pmatrix} \psi_1 \\ \psi_2 \\ \psi_3 \end{pmatrix} = \begin{pmatrix} c_{11} & c_{12} & c_{13} \\ c_{21} & c_{22} & c_{23} \\ c_{31} & c_{32} & c_{33} \end{pmatrix} \begin{pmatrix} wv^2 \\ wv \\ 1 \end{pmatrix} \quad (12)$$

Where, c_x are the coefficients taken from the Jiménez-Muñoz et al., 2014.

k) Applying minimum temperature filter

After the estimation of LST a minimum temperature (20°C) filter was applied to avoid the cloud contamination which was undetected by cloud mask.

l) Extracting the data from processed Landsat images for further analysis

From the processed LST, each image's minimum, mean and maximum LST values were extracted for further analysis. The LST values are put together in a data frame, including the time of acquisition and sensor information (Table 2).

Notably, among all these steps and processing described here, only processed LST, Spectral indices and extracted statistics (mentioned in the next paragraph) are used and presented in the results. All the immediate steps were necessary for LST estimation and are not interpreted in the result section.

Table 2: Example of extracted data from processed Landsat images

	MeanLST	MaxLST	MinLST		Timestamp	Year	Month	Day	DOY	Sensor
0	25.760589	32.832072	20.374920	2000-01-06 02:55:05.105	2000	1	6	6		LS5
1	24.394343	32.779574	20.000007	2000-01-22 02:54:43.225	2000	1	22	22		LS5
2	34.390964	44.140048	29.395546	2000-02-23 02:53:34.645	2000	2	23	54		LS5
3	31.308242	39.882945	26.932541	2000-03-10 02:53:30.594	2000	3	10	70		LS5
4	32.094862	40.587537	24.399067	2000-03-18 03:12:36.882	2000	3	18	78		LS7
...
457	25.436674	36.283008	20.004712	2021-08-11 03:20:08.962	2021	8	11	223		LS8
458	26.783289	40.003087	21.471625	2021-10-30 03:20:27.347	2021	10	30	303		LS8
459	29.779328	46.981748	21.349140	2021-11-07 02:12:42.366	2021	11	7	311		LS7
460	NaN	NaN	NaN	2021-11-15 03:20:22.543	2021	11	15	319		LS8
461	22.040610	36.152164	20.001485	2021-11-23 02:11:08.380	2021	11	23	327		LS7

2.4.2 LST ranges, seasonal variation, and trend analysis

A descriptive analysis is performed where the descriptive statistics like the number of observations and minimum, mean, median, and maximum values are observed and

compared in terms of minimum, mean and maximum LST. Box-whisker-plot is produced to illustrate the LST data distribution.

Calendar heatmaps are used, which provide information about seasonal trends, yearly comparison of LST distribution, anomalies and extreme events and consistency of the temperature range. To understand the consistency of the LST range, minimum and maximum LST for every year were visualised together in a box-whisker-plot.

An arbitrary scale was applied to conduct a yearly comparison based on comparatively warmer months each year (Table 3). The reason for choosing such an approach is to understand which years are comparatively warmer between 2000 and 2021. A warmth score is calculated based on the number of warmer months in a year. For example, the year 2000 has 03 months with equal or more minimum LST than 28 °C, 05 months with equal or greater mean LST than 32 °C and 05 months equal or more maximum LST than 42 °C. Hence, the warmth score of 2000 is 13 (03 + 05 + 05). A stacked bar chart represents this yearly comparison of warmer months in different LST categories and warmth scores.

Table 3: Scale for the identifying comparatively warmer months

Category of LST	LST (in °C)	Remarks
Minimum LST	≥ 28	Comparatively warmer months
Mean LST	≥ 32	
Maximum LST	≥ 42	

Images from every month in 2015 are presented together to get an impression of the seasonal variation of LST. The year 2015 was selected for this because this year had cloud-free data. To understand the seasonal variability in terms of number, the minimum, mean, and maximum LST is presented together as a point chart from 2015.

Trend analysis was conducted by plotting simple line charts of minimum, mean and maximum LST. It is important to note here that April to October 2011 has missing data where a linear method interpolation is applied to ensure continuity in the trend analysis (Burden et al., 2015). In addition, line charts and error bands for minimum, mean, and maximum LST are also produced. The error bands represent the Interquartile Range (IQR), a measure of statistical dispersion or the middle 50% of values when ordered from lowest to highest.

One LST image from each year is visualised together, where all the images are taken from February to April to ensure coherence in seasonal fluctuation. While images from the same day of each year would be better for such comparison, it was not possible

because of different image acquisition dates and the cloud presence. However, from this visual representation, five consistently warmer areas are identified as the hotspots.

2.4.3 LST vs LULC relationship analysis

The relationship between LST and LULC was assessed both visually and quantitatively. For visual assessment, LST values, including their timestamps, are extracted to see the distribution of LST from 2000 to 2021 at the identified five hotspots (Table 4). Only the month of March from every year was considered to avoid the seasonal influence. At the same time, images from Google Earth from a similar timeline were observed to compare and understand if there is any visible connection between the changes in LST values and changes in LULC. This report presented three of five identified hotspots in point charts with a linear trend line and related Google Earth images.

Table 4: Example of the extracted data for visual LST vs LULC relationship analysis

LST1	LST2	LST3	LST4	LST5	Timestamp	Year	Month	Day	DOY
29.652098	31.672999	28.882752	32.498476	NaN	2000-03-10 02:53:30.594	2000	3	10	70
NaN	NaN	31.579005	NaN	NaN	2000-03-18 03:12:36.882	2000	3	18	78
33.635402	NaN	NaN	31.396561	34.968446	2000-03-26 02:54:16.973	2000	3	26	86
37.511851	37.579708	NaN	NaN	NaN	2001-03-29 03:00:11.171	2001	3	29	88
36.235501	41.630416	36.145998	42.231825	39.163778	2002-03-08 03:08:57.240	2002	3	8	67
NaN	NaN	NaN	40.957689	NaN	2002-03-24 03:08:50.300	2002	3	24	83
41.705534	46.860264	40.241426	42.725183	52.081739	2003-03-27 03:08:40.340	2003	3	27	86
NaN	NaN	NaN	38.094707	NaN	2004-03-05 02:59:02.420	2004	3	5	65
42.636720	NaN	38.255287	NaN	NaN	2004-03-29 03:09:18.190	2004	3	29	89
35.693140	NaN	31.862696	38.075748	32.382502	2005-03-08 03:06:54.330	2005	3	8	67
42.899950	NaN	36.330448	42.803600	NaN	2005-03-16 03:09:43.750	2005	3	16	75
NaN	NaN	NaN	NaN	NaN	2006-03-03 03:10:07.360	2006	3	3	62
34.869531	37.493470	NaN	37.415895	33.942154	2006-03-11 03:11:04.290	2006	3	11	70
37.788100	46.219406	34.463868	38.372780	NaN	2007-03-06 03:10:31.890	2007	3	6	65

A correlation test was performed to quantitatively understand the relationship between LST and LULC. For this purpose, four hundred random points were drawn within the study area (Figure 6). On these 400 random points, values of LST and the spectral indices (IBI, MNDWI and NDVI) were extracted and put together into a data frame (Table 5). Pearson's Correlation Coefficient was determined to understand the magnitude of the relationship between these parameters (Pearson, 1920).

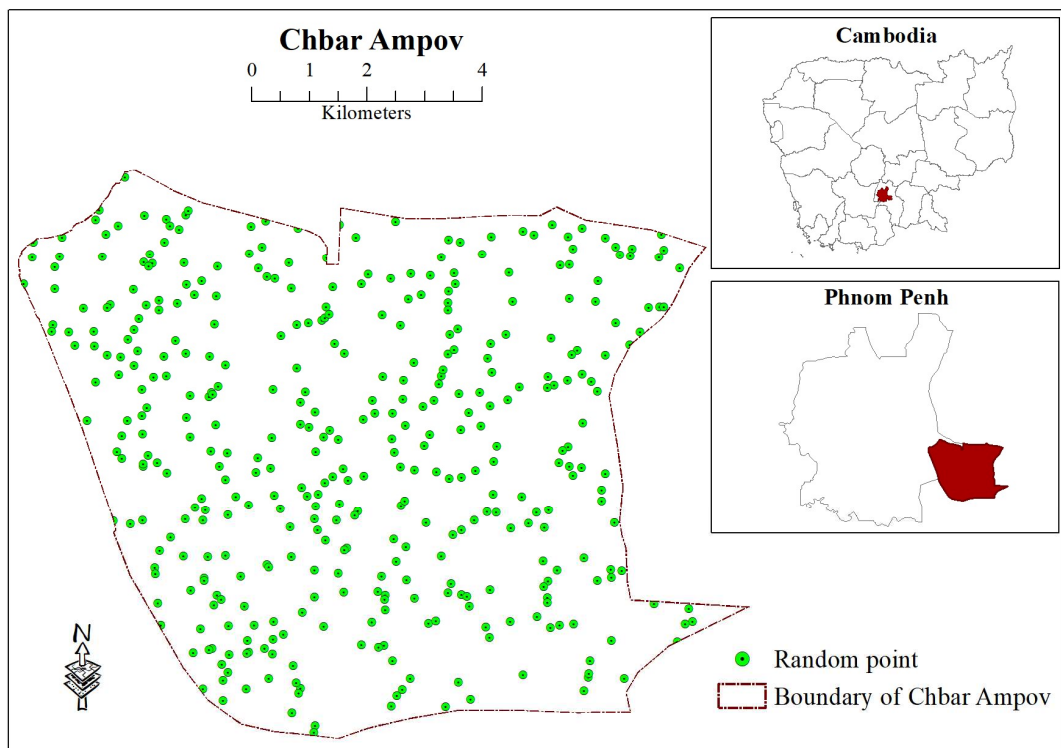


Figure 6: Location of random points for correlation test

Table 5: Example of the extracted data for correlation test

	id	LST	NDVI	IBI	MNDWI
0	0	39.40906	0.54235	-0.11570	-0.42295
1	1	36.36639	0.58471	-0.09169	-0.45279
3	3	41.70393	0.32306	-0.08670	-0.23359
6	6	41.66842	0.58582	-0.11779	-0.45501
7	7	40.46561	0.55696	-0.09691	-0.45548
...
394	394	37.99087	0.60943	-0.12744	-0.44707
395	395	39.74504	0.60094	-0.09669	-0.48521
396	396	37.89942	0.69099	-0.20500	-0.44331
397	397	38.94889	0.40980	-0.00817	-0.43910
399	399	36.36948	0.62431	-0.12719	-0.46234

3 Results

This section presents the results and interpretation of LST values, focusing on descriptive statistics, calendar heatmaps, LST trends, and the relationship between LST and LULC. This section provides insights into the distribution and variability of LST and its relationship with various elements such as seasonal trends, anomalies, extreme events, and LULC changes. Additionally, this section examines the correlation between LST and spectral indices representing different LULCs. The findings shed light on the interaction between LST and LULC, enhancing understanding of the thermal dynamics shaping the local environment and climate.

3.1 Overview of LST distribution and ranges during 2000 - 2021

Among the total 425 images, the distribution of LST values varies across the three categories of LST, namely minimum, mean and maximum LST (Table 6). The Minimum LST has the narrowest range, while the Maximum LST exhibits the broadest range, indicating a wider spread in extreme temperature values. The Mean LST has a relatively more considerable standard deviation than the Minimum LST, suggesting a wider dispersion of average temperatures. Notably, the median values for all three datasets are relatively close to their respective means, which could imply that their distributions are roughly symmetric and not heavily skewed, and this can be visually observed by the following box-whisker plots (Figure 7).

Table 6: Descriptive statistics of minimum, mean & maximum LST

	Minimum LST	Mean LST	Maximum LST
Count*	425	425	425
Minimum	20.00	20.41	20.54
Mean	24.34	30.85	43.25
Median	22.83	30.79	43.88
Maximum	37.29	50.95	69.40
Std Dev**	4.54	5.58	8.57

* The original number of observations was 462, after removing a miscalculation in LST it became 461. However, the data contains 36 missing values. Hence the count is 425.

** Standard deviation

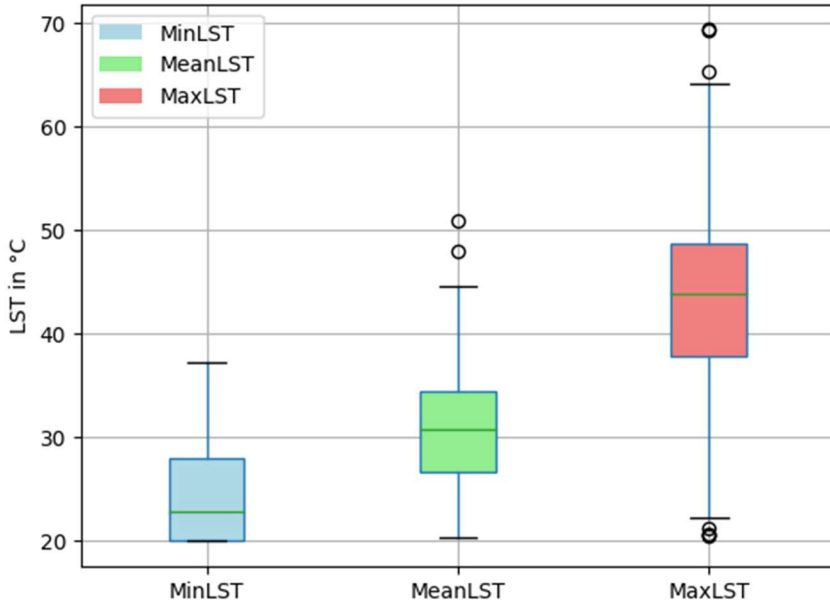
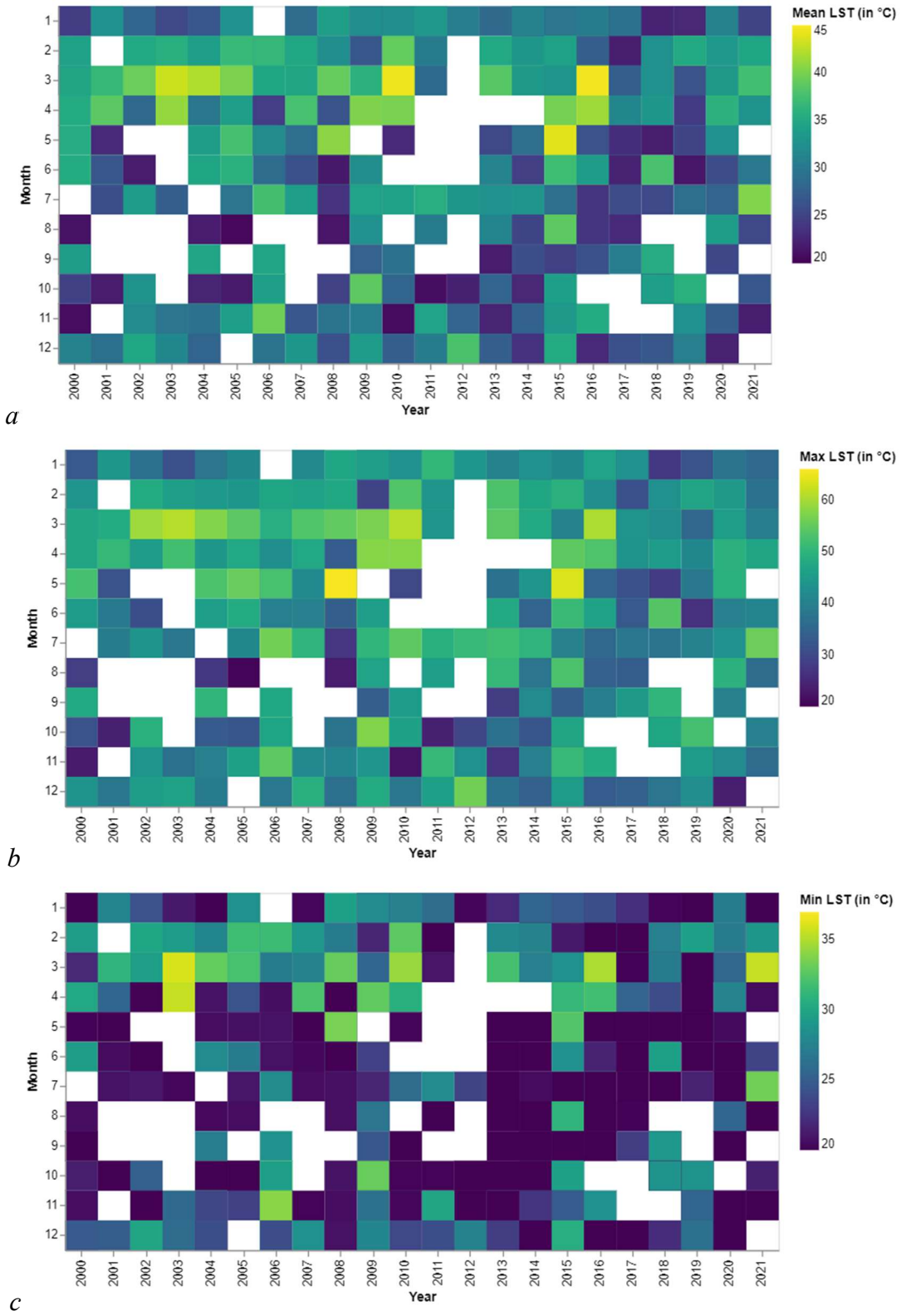


Figure 7: Boxplot of minimum, mean & maximum LST

The above box-and-whisker plot describes the distribution of the LST in these categories (minimum, mean and maximum) (Figure 10). The presence of outliers in the mean LST and maximum LST datasets implies that a few extreme values deviate widely from the central tendency of the respective categories. In the case of mean LST, outliers above the range could represent unusually high average temperature values compared to the overall distribution. For maximum LST, outliers above the range could indicate exceptionally high maximum temperatures, while outliers below the range could signal shallow maximum temperatures.

The calendar heatmaps are created to get a temporal overview of the LST (Figure 8). It is worth mentioning that the minimum, mean, and maximum LST scales are different because it is difficult to visualise the difference in all three categories using a single scale. The heatmaps show that LST is comparatively higher from November to April, indicating the area's dry season. Among these months, February to April consistently showed higher LST in all three categories (Minimum, Mean and Maximum). However, in some months and years, May (the month) also has higher temperatures. The rest of the months (June to October) have lesser LST, apart from a few exceptions in specific years and months. Mean LST has four high values, three of which are in March 2003, 2010 and 2016, where the values are 43.10°C , 44.43°C and 44.58°C . The fourth value was on May 2015 (43.86°C). While it requires more extended period data to say it concretely, these anomalies appear every sixth or seventh year during the dry season.



*Figure 8: Calendar heatmaps of LST. a. mean, b. maximum & c. minimum
(All the white blocks in these figures represents the no data)*

Annual ranges of LST are presented on the following box-whisker-plot (Figure 9). There is an apparent interconnection between the minimum, mean, and maximum LSTs: as the minimum LST rises, there are usually corresponding increases in the mean and

maximum LSTs. This influence of minimum LST is expected, as higher minimum temperatures in a given year would push the average and potentially influence the maximum temperature.

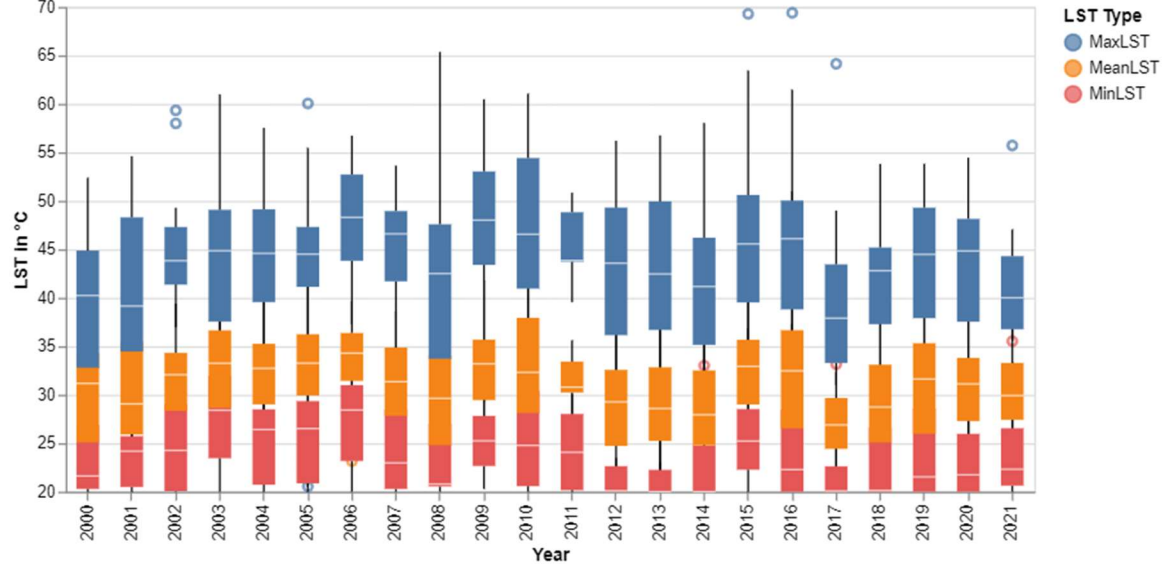


Figure 9: Annual LST range

It also observed that the 75% quartile for maximum LST appears to have a rising trajectory across the years, suggesting that the warmest 25% of temperatures are experiencing an increase. This rise was particularly noticeable in 2006, which shows a significant increase in maximum LST's 75% quartile compared to previous years. Similarly, if we look at the 25% quartile for minimum LST, we see a general trend of increasing values over time. This increase of 25% quartile of minimum LST suggests that the coldest 25% of temperatures are becoming less cold over the years, which is prominently visible in 2003.

There appears to be a cyclical behaviour with peaks and troughs in mean LST occurring every few years. For instance, a peak in mean LST appears in 2006, followed by a trough in 2007, indicating possible cyclical patterns in the weather.

Outliers are observed in several years, typically indicating unusually high maximum LST in 2002, 2015, 2016, 2017 and 2021. Similarly, there were unusually high mean LSTs in 2014, 2017 and 2021. On the contrary, unusually low maximum LST was observed in 2005 and low mean LST in 2006. While these insights provide a general overview of the annual LST distribution and ranges in different LST categories, they do not give the impression of which years were comparatively warmer.

A threshold for each LST category is used to identify comparatively warmer years. The threshold values are 28 °C or higher for minimum LST, 32 °C or higher for mean LST and 42 °C or higher for maximum LST (c.f. Section 2.4.2, Table 2).

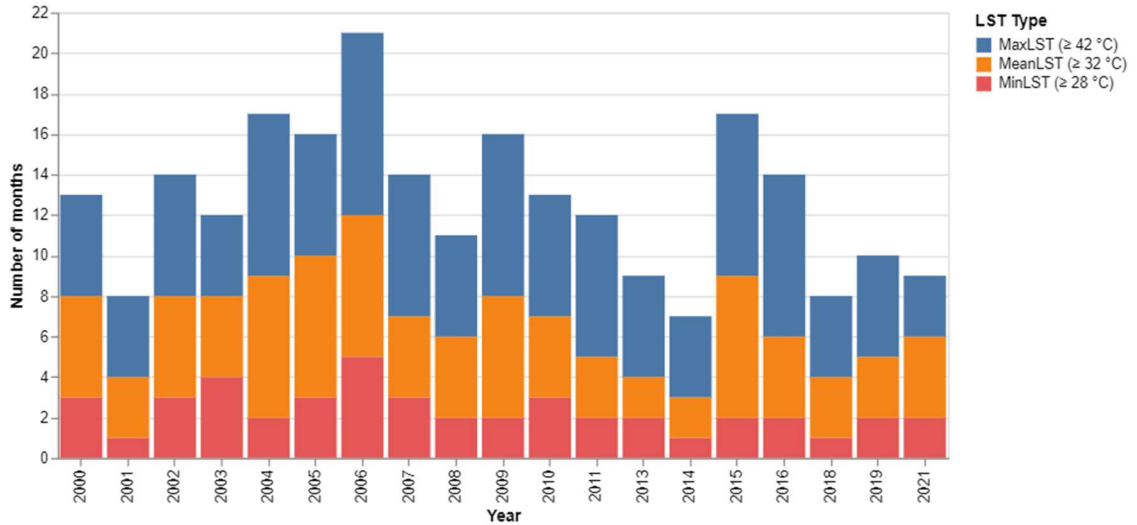


*Figure 10: Number of warmer months per year in LST categories
The height of each bar represents the warmth score for respective years.*

The yearly comparison based on the set threshold values shows that in terms of minimum LST, 2000, 2002, 2003, 2005, 2006, 2007 and 2010 are comparatively warmer (Figure 10). In terms of mean LST, 2004, 2005, 2006, 2009, and 2015 are comparatively warmer, and 2004, 2006, 2009, 2011, 2015 and 2016 are the warmer years in terms of maximum LST. The warmth score is created from the simple addition of the number of warm months and is represented by the bars (Figure 10). Based on the warmth scores, 2004, 2006, 2009, and 2015 appear to be comparatively warmer years.

3.2 Seasonal variability of LST

From the above results and interpretation, it is evident that there is a seasonal influence over the LST. Image from different months from the same year is observed to understand this seasonal variation. Apart from that, there are irregularly warmer months in different years in these heatmaps. To illustrate this variation in the heatmaps, maps from all months in 2015 have been visualised together to understand the seasonal variation (Figure 11).

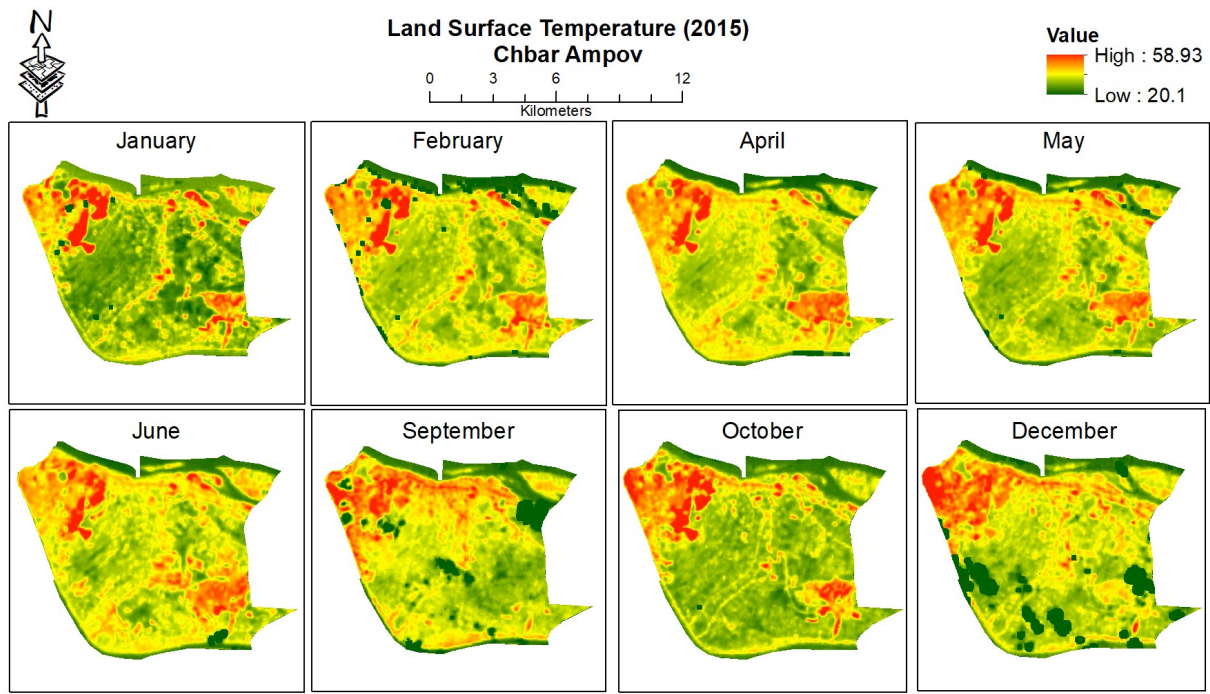


Figure 11: Spatial-seasonal variation in LST

More cloud-free images needed to be visualised for March, July, August and November. There is a seasonal variability of LST as it shows different ranges and distributions of LST within different months of the same year. For example, a noticeable difference between January and April is also reflected similarly in the heatmaps. These images' minimum, mean, and maximum LST values are visualised to understand this variability (Figure 12).

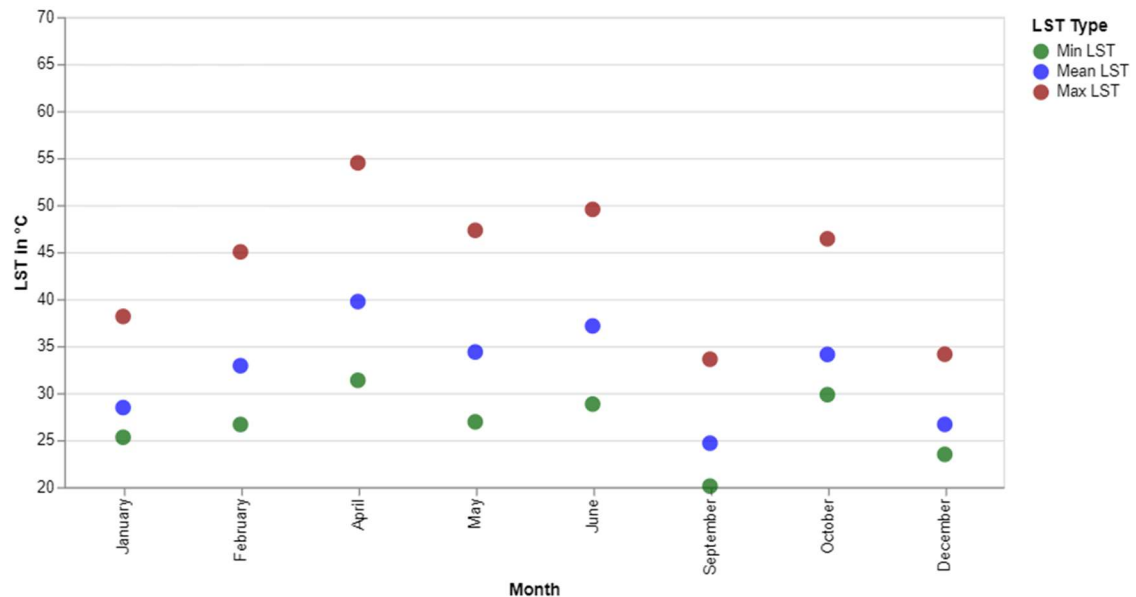


Figure 12: Monthly minimum, mean and maximal LST in 2015

There is quite a fluctuation between different months in the same year regarding minimum, mean and maximum LST. The maximum difference in all the values appears

between April and September. All the LST values are lower in September, which are comparatively higher in the immediate next month (October). Apart from seasonal influence or variation, one reason is the presence of clouds in the places where the higher LST is consistently visible in other months (Figure 13).

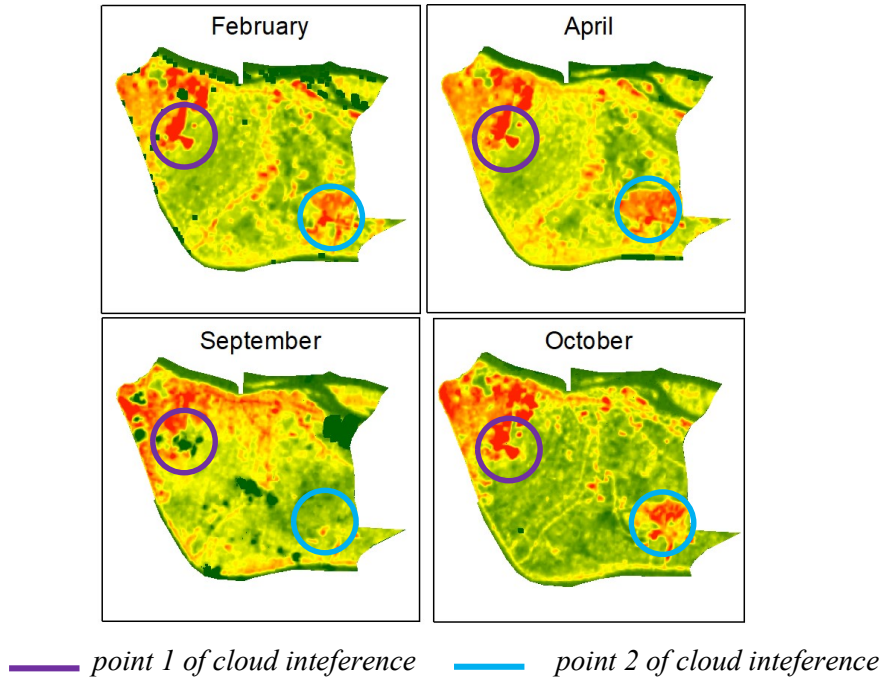


Figure 13: Example of unusual monthly fluctuation in LST

Also, a higher temperature patch is visible in the southeast in all other months except September. This is to understand the more realistic variability between the months of a particular year (2015). The difference between April and October has been considered in this study. There are two reasons behind choosing these two months. Firstly, both are entirely cloud-free, which enabled a good comparison, and the difference between the two months is apart enough to represent different seasons in this area. Between April and October, the difference in minimum, mean, and maximum LST is 1.53, 5.62 and 8.08 °C, respectively. This seasonal variability is essential to understand the long-term trend of LST, especially when data from different seasons are considered.

3.3 Trend of LST and hotspots identification

The following line chart represents the minimum, mean and maximum LST trend from 2000 to 2021(Figure 14). The 20 °C flatline at the bottom is due to the temperature filter used on the data. The maximum temperature is usually below 60 °C apart from a few years such as 2008, 2015, 2016 and 2017. Regular fluctuation exists due to the seasonal variation explained in the previous section (cf. section 3.2). However, the noticeable

temperature spikes in each category seem symmetrical. When the maximum temperature spiked, the mean and minimum also seemed to peak in most cases.

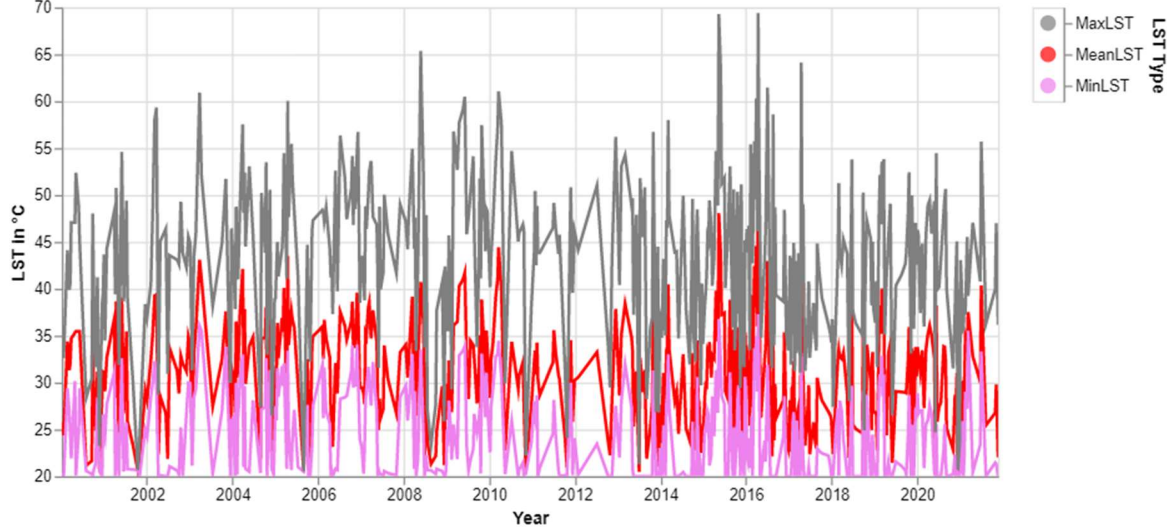


Figure 14: Total time series of minimum, mean & maximum LST (2000 - 2021)

The distribution of LST by year is represented as an interquartile range envelope, and the median line is presented (Figure 15).

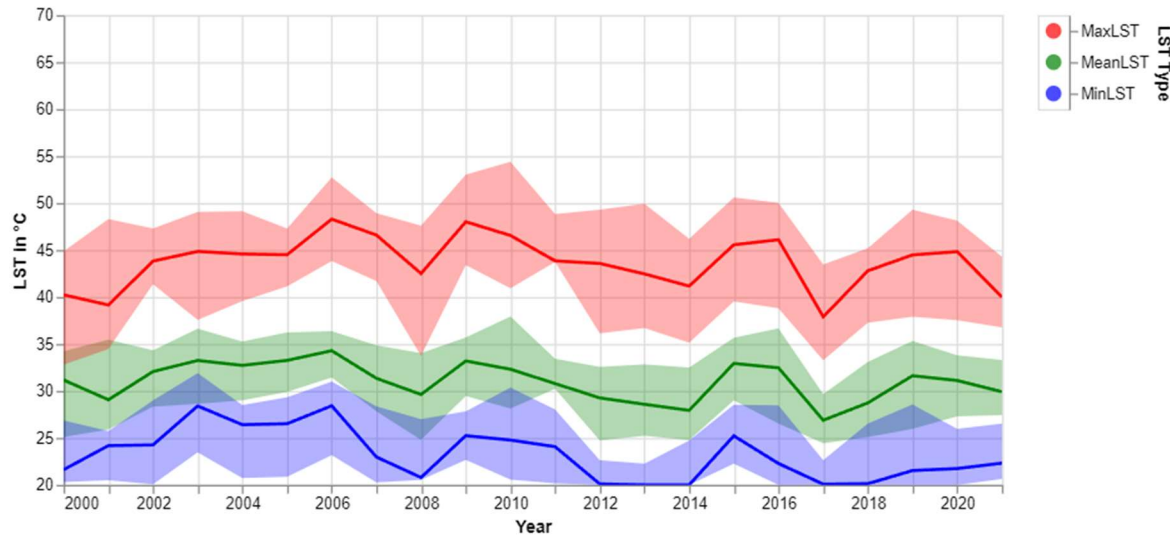


Figure 15: Time series with error bands chart of LST

The spread of the data in the quartile chart helps reveal how the data is distributed and highlights any potential outliers. The chart above represents the median value and an error band showing the interquartile range (IQR). The IQR is the range between the first quartile (25th percentile) and the third quartile (75th percentile), thus visually representing the central 50% of the data. However, no long-term trend of LST is visible in all three categories.

The changes in LST during study period is observed visually below (Figure 16). This representation provides an overview of a few things. It shows how LST has changed in

some areas, specifically in the northwest and southeast, over the period. An increase in the northeast can be linked to the urban expansion of Phnom Penh City. The southeast part of the study area has gone through the construction of a golf course from 2015 onwards. This means a visible connection between LULC and LST. This connection or relationship is explained more elaborately in the next section.

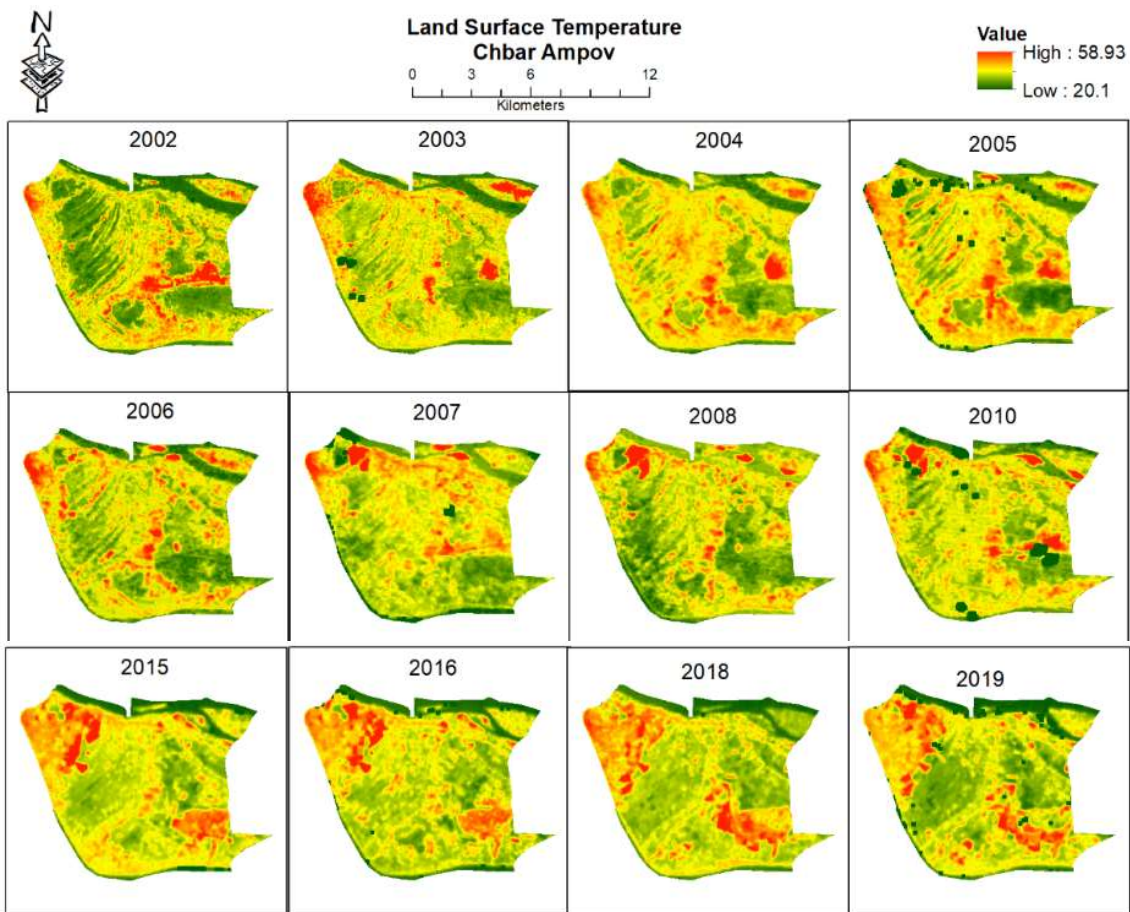


Figure 16: LST in 2000 - 2021

Some specific points in Figure 19 appeared that contain consistently higher LST, identified as hotspots based on visual observation (Figure 17).

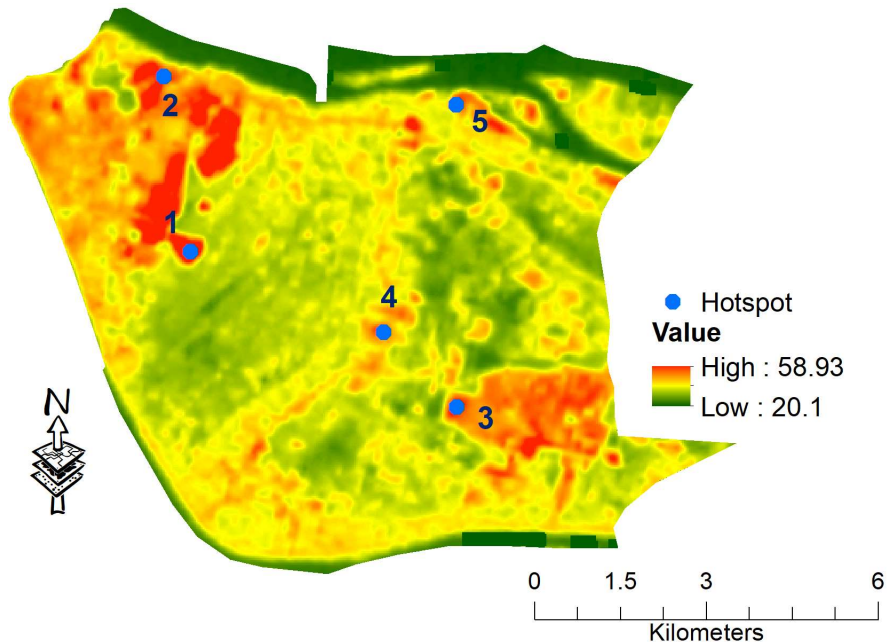


Figure 17: Location of identified 5 hotspots (background map is from April 2015)

3.4 Response of LST to different LULC in identified hotspots

LST data is extracted over time to observe the changes in LST to look further at these hotspots on three out of five points. At the same time, to understand these changes, images from Google Earth are used to see if there is any visible relation to the LULC changes with LST change.

The first point was a wetland around 2003 which was mostly covered with shrubs (Figure 18). In 2011 the water somehow got exposed; thus, a downward spike in the temperature was noticed. The most apparent LULC shift was noticed in 2015 when landfilling was initiated, and in 2016 when it was utterly exposed, land shows the highest LST in the considered timestamps. Overall, there is an upward trend of LST at this particular point.

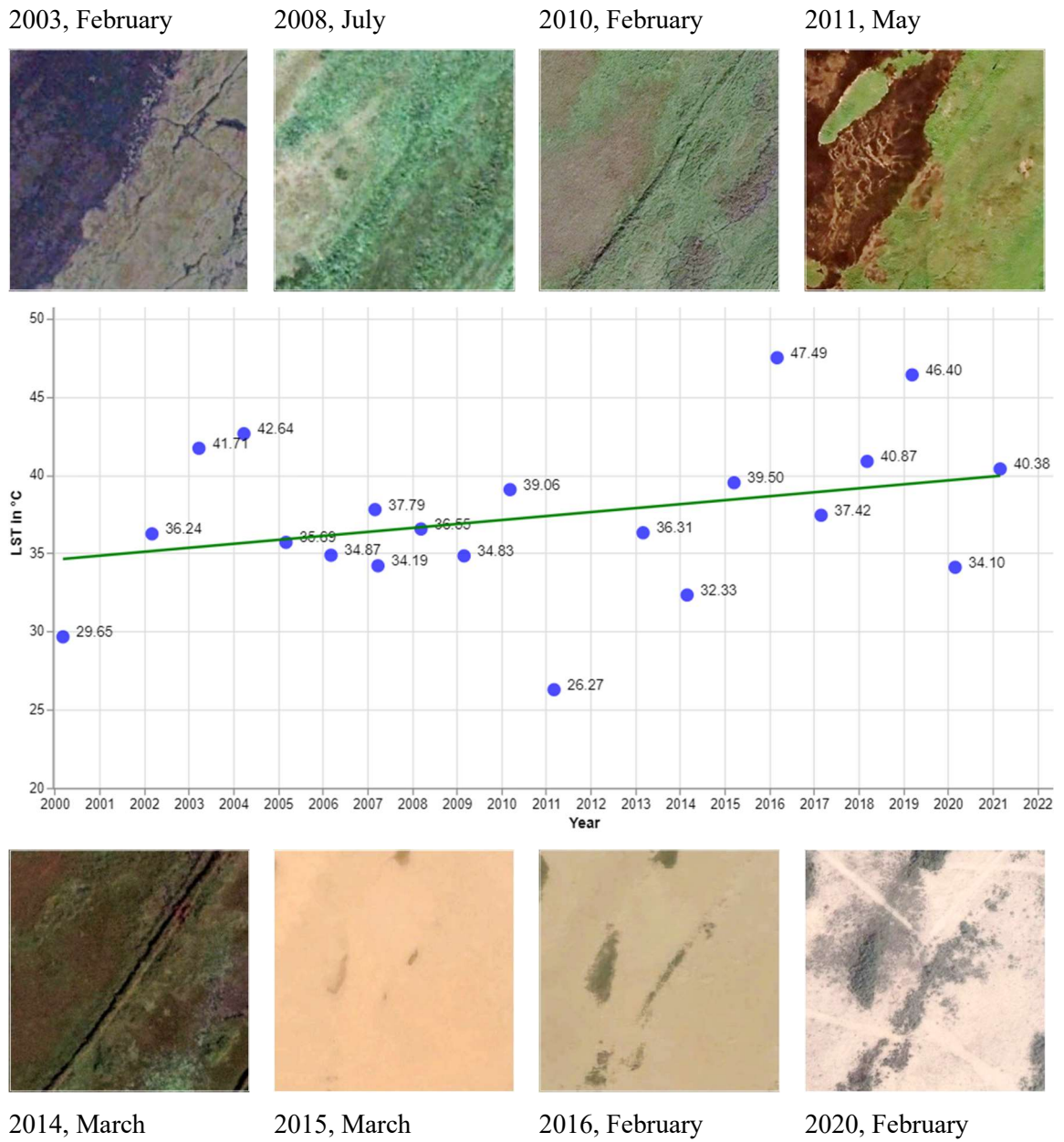


Figure 18: LST and LULC changes in point 1

The second point started partially as a wetland and unused exposed land around 2003 (Figure 19). The wetland part was filled around 2008, thus the upward spike in LST. Around 2011 the area was mostly covered with bush. Another upward spike in the LST occurred in 2016 when a settlement was built. The area had dense vegetation in 2018, and LST decreased compared to 2016. Then in 2021, the settlement was no more there, leaving the place bare of soil and partially covered with bush, where the LST increased compared to 2018. There were fluctuations in LST occasionally but no visible long-term trend in this area.

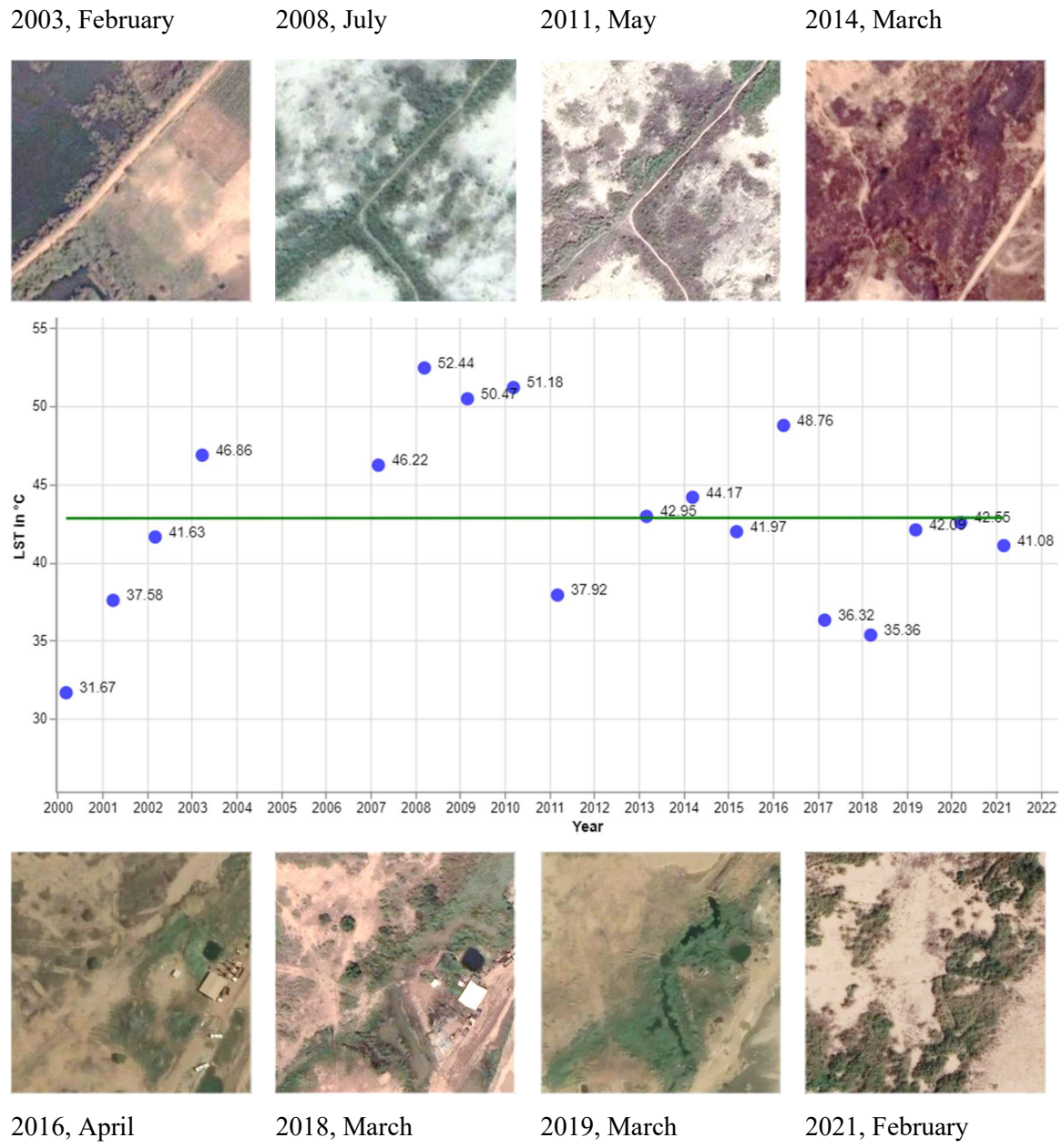


Figure 19: LST and LULC changes in point 2

The third point has undergone notable LULC and LST changes (Figure 20). The area was agricultural land with some vegetation and a small waterbody in 2003. By 2008 the area became lush green with several trees and dense vegetation, which was reflected by the downward spike of the LST. However, by 2010 the area lost all the trees and vegetation and, thus, an upward spike in LST. The area showed the highest LST in 2016 when the area contained a large building and mostly exposed soil. Overall, the area shows an upward trend in LST.

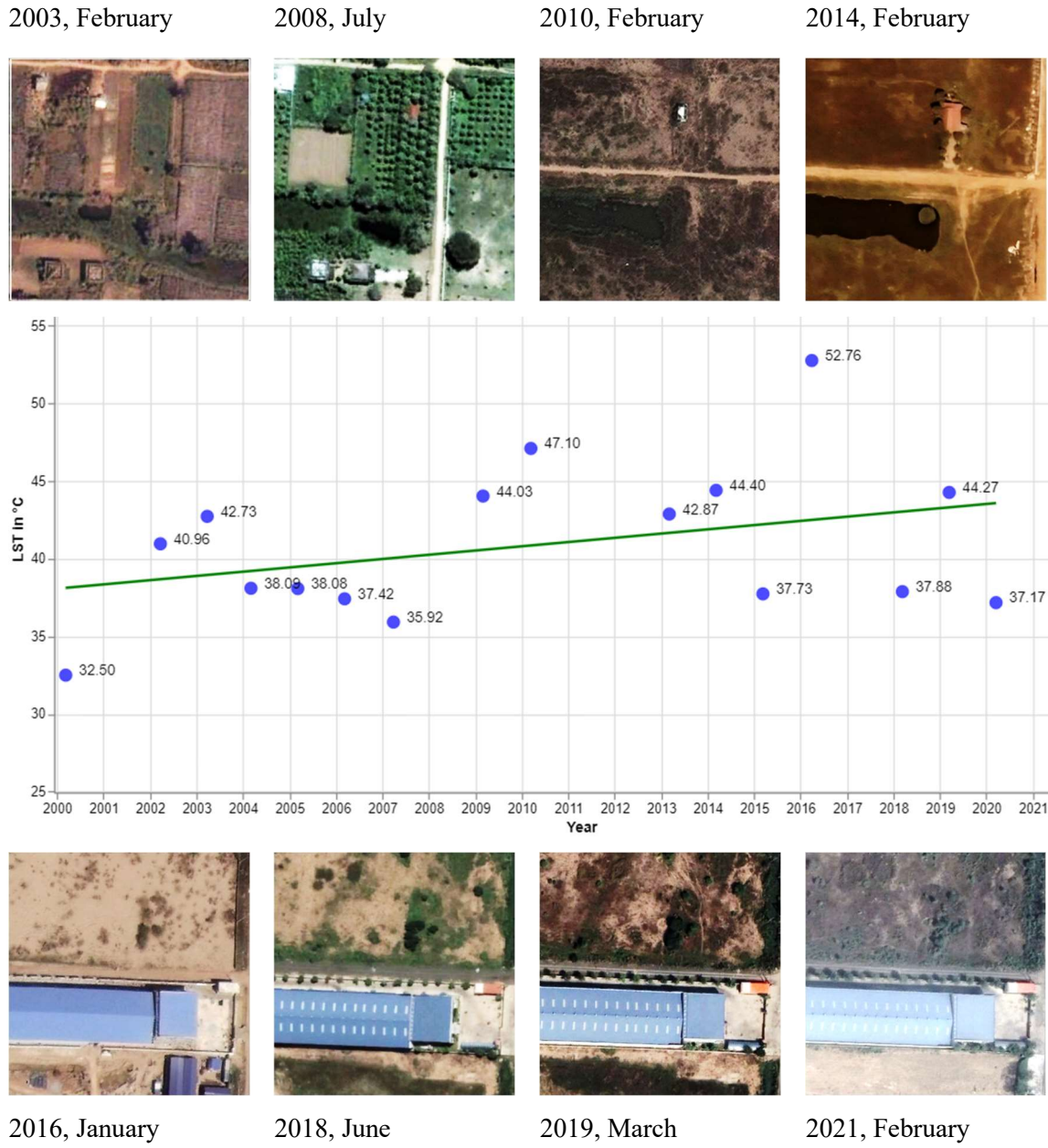


Figure 20: LST and LULC changes in point 3

The representation of LST changes and comparison of LULC changes shows a visual connection between LST and LULC changes. However, this connection is from a visual interpretation that does not tell any specific quantitative information about this relation or explain its intensity. Hence, in the next section, this relationship is tested quantitatively using a correlation test between LST and different spectral indices values representing the typical land covers (Vegetation, water, and built-up areas).

3.5 Correlation between LST and different land covers

The descriptive values that have been analysed so far helped get an overview of LST distribution and changes. However, they are not helpful for a correlation test because they represent different points in every value for a single observation. Hence, the

correlation test is performed from the randomly generated 400 points (cf. section 2.4.3). A correlation matrix is generated to understand the correlation between different parameters, including LST, IBI, MNDWI and NDVI (Figure 21).

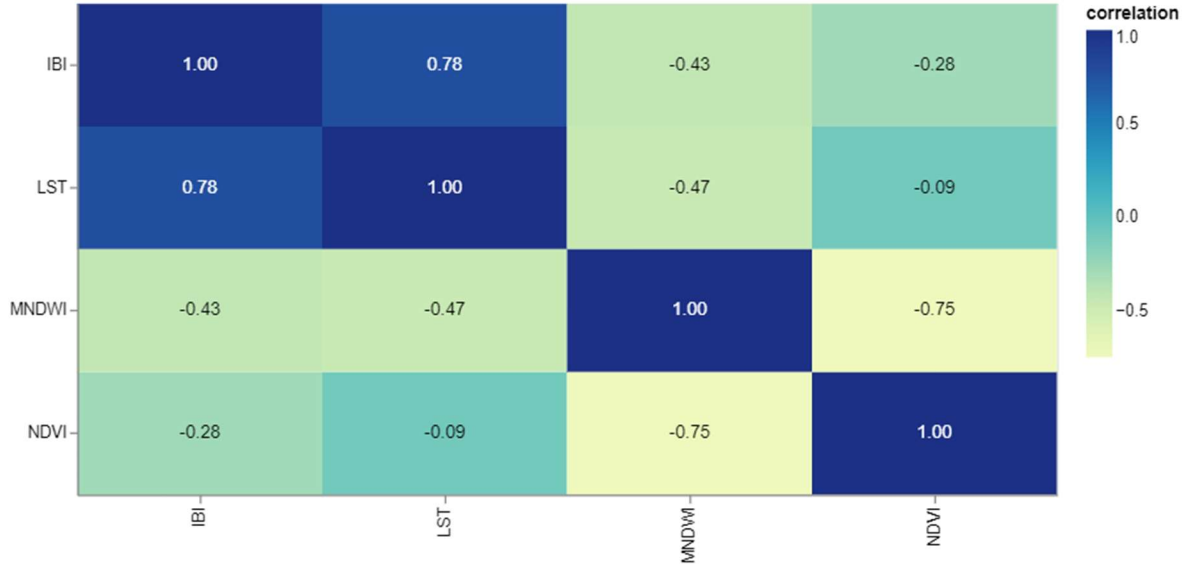


Figure 21: Correlation matrix between LST, IBI, MNDWI & NDVI

The correlation matrix indicates a strong positive correlation between the built-up area and LST. This relationship appears to be linear (Figure 22). This explains the increase of LST over the year in the northwest and southeast part of the study area.

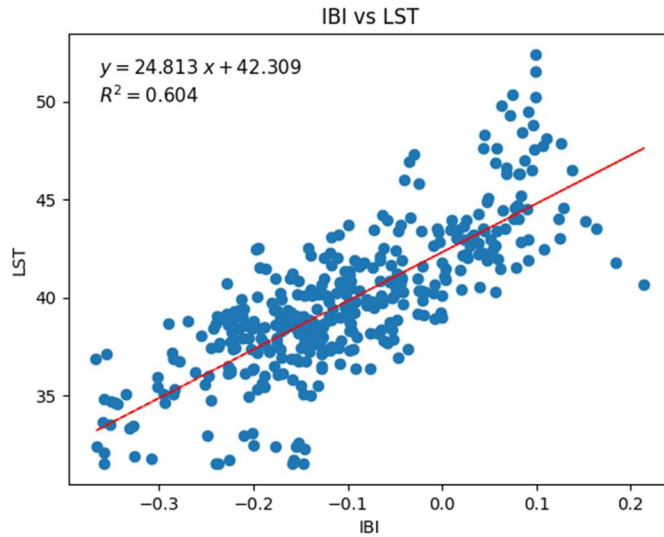


Figure 22: Linear relationship between built-up area and LST

However, this matrix does not accurately represent the relationship between LST, MNDWI, or NDVI. Because in the vegetation pixels, both MNDWI and LST values are less, which creates a contradiction in expressing the relationship (Figure 23a). Without the vegetation pixels, it is observed that there is a strong negative correlation between LST and water (Figure 23b).

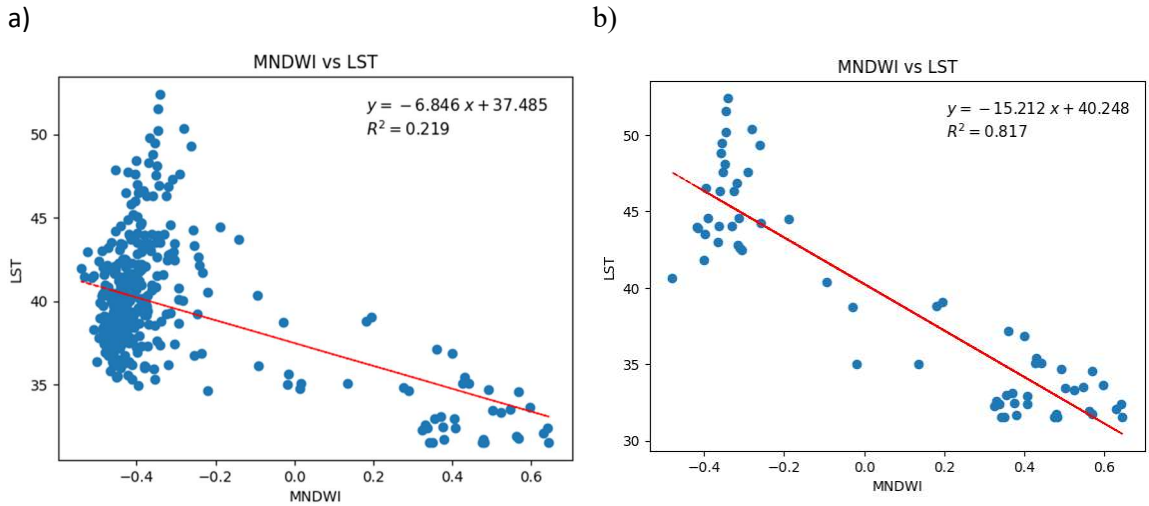


Figure 23: Relationship between water and LST;
a) including vegetation pixel, b) without vegetation pixel

Similarly, the lowest value of NDVI represents water with lower LST. Hence this can create a similar contradiction in the relationship between LST and NDVI (Figure 24a). So, only the vegetation pixels (≥ 0.2 NDVI) were used to assess the relationship between LST and NDVI (Figure 24b). LST and vegetation have a strong negative correlation between them.

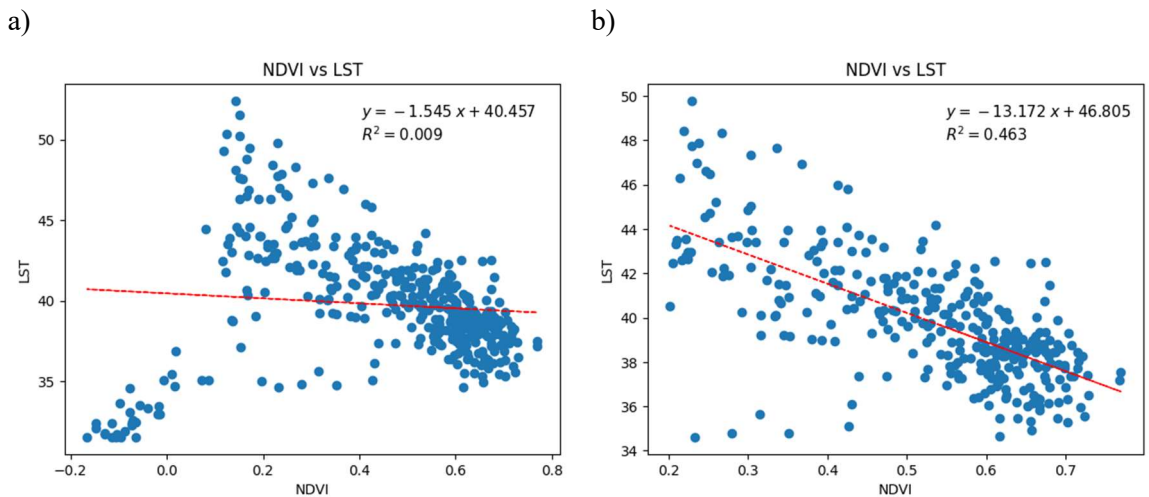


Figure 24: Relationship between vegetation and LST;
a) including all pixel, b) only vegetation pixel

Considering the contradictions mentioned above, a revised correlation matrix is prepared, representing the correlation between LST and these spectral indices more accurately (Figure 25). In this matrix, the relationship between LST and MNDWI is considered without the vegetation pixel and for LST and NDVI, only vegetation pixels are considered.

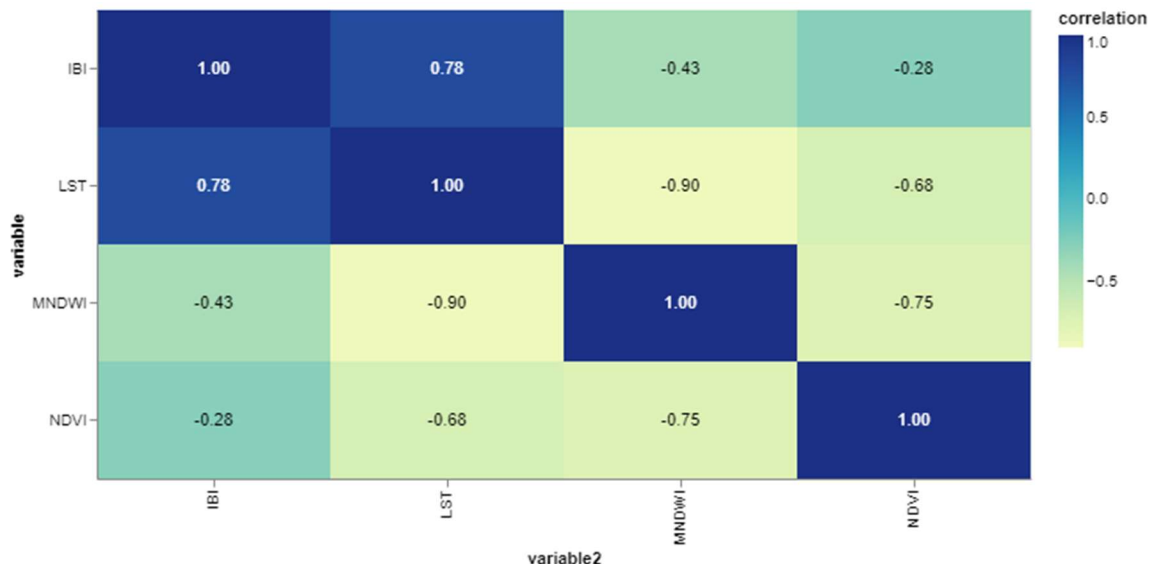


Figure 25: Revised correlation matrix between LST, IBI, MNDWI & NDVI

4 Discussion

4.1 Overview of the study objectives and the key findings

The study aimed to examine the spatiotemporal patterns of LST in the study area of Chbar Ampov and to investigate the relationship between LST and LULC changes using remote sensing techniques. The study also aimed to analyse seasonal variability, LST trends, and the response of LST to different LULC types in specific hotspots. Key findings from the study include a noticeable seasonal influence on LST, with the maximum difference in values occurring between April and September. While the study found fluctuations in LST, no long-term trends were visible in the data. The study also identified hotspots with consistently higher LST values and found a visual connection between LST and LULC changes in these areas. A strong positive correlation between built-up areas and LST was observed, while a strong negative correlation between LST and water was found. The correlation between LST and vegetation was found to be moderately strong.

4.2 Discussion on data and methods

Before we discuss about data and methods used in this study, it is essential to discuss the distinction between LST and air temperature. They represent distinct physical phenomena and are measured in different ways. Air temperature is gauged approximately 1.2 meters above ground level, differentiating it from LST. However, a study suggested that the increase in LST and air temperature are parallel (Aniello et al., 1995). Another study asserts that air temperature and LST patterns are interchangeable (Saaroni et al., 2000). This proposition was examined in a subsequent study, which

argued that LST showed greater local variability when compared to air temperature (Nichol et al., 2009). In addition, Saaroni et al. (2000) argued that while air temperature provides information for a specific point or transect, LST provides a continual depiction of temperature, which offers more valuable insights into temperature patterns. However, air temperature and LST can complement each other to produce a better accurate interpretation of thermal dynamics.

A combination of data from different sensors was needed to build the timeline of this study. However, this combination of sensors also requires specific issues to consider during analysis. In the case of Landsat, all the sensors have a 16-day revisit schedule according to their timeline. Hence, obtaining images from the same day of each season and year is only possible in some cases when it comes to different sensors. Landsat 5 has a spatial resolution of 120 m in the thermal band, which is 60 m for Landsat 7 and 100 m for Landsat 8. While all the thermal bands are re-sampled into 30m pixel resolution due to their inherent difference in their actual spatial resolution pixel to pixel comparison lacks a certain degree of coherence.

The Scan Line Corrector (SLC), a component of Landsat 7 ETM+, failed on May 31, 2003. As a result, instead of scanning a continuous swath of the Earth's surface, the sensor began to capture a series of parallel scans with gaps in between (Storey et al., 2005). This failure of SLC resulted in a pattern of data gaps or "stripes" in each Landsat 7 scene, affecting the quality and usability of the satellite's data. However, Landsat 7 continued to capture data and techniques have been developed to fill the data gaps using information from overlapping images or other sources to produce SLC-off gap-filled products (Scaramuzza et al., 2004). The Landsat 8 experienced unanticipated calibration inconsistencies of one of its thermal infrared sensor bands - Band 11 that impacted the data's accuracy creating a bias in the recorded land surface temperatures (Montanaro et al., 2014). These kinds of technical issues are also critical aspects of building a timeline using the data from these sensors.

There are several algorithms and techniques to estimate LST from Landsat data. The study used the single-channel algorithm considering the sensor variation because it requires only one thermal band (Jiménez-Muñoz & Sobrino, 2003). Since Landsat 5 and 7 have only one thermal band, it was the ultimate choice to perform the time series using Landsat 5, 7 and 8 together. However, it needs to consider the atmospheric information and emissivity values of the primary surfaces that are being inspected. These parameters can influence the accuracy and quality of the output LST data. If the

local atmospheric data is available radiative transfer equation (RTE) algorithm can be an alternative for a high degree of accuracy (Du et al., 2015). If the study duration can be covered by the sensors that have more than one thermal band split-window algorithm can be a better choice over the single-channel algorithm because this technique is better at dealing with the atmospheric effects, especially in humid areas (Sobrino et al., 2008). Because of the difference between sensors and technical issues and differences in methods, while the representation of LST can indicate trends and patterns efficiently, the absolute temperature values used in results should be less accurate measurements.

4.3 Discussion on results

The seasonal influence on LST was evident, with substantial differences between various months within the same year. This result aligns with the study conducted by Weng (2001) and Zhou et al. (2014). This finding highlights the importance of considering seasonal variability when analysing long-term trends of LST, mainly when data from different seasons are being used.

While quantitative analysis is meaningful to understand the statistical significance, it is also essential to have a visual interpretation. Otherwise, we may miss certain pertinent information, thus leading to misinterpretation of the thermal dynamics. Despite fluctuations in LST, no long-term trends were observed in the data. This finding implies that while LST can vary seasonally, there is no clear evidence of an overall increase or decrease in LST over the study period. Further research might be needed to investigate the factors contributing to this lack of a long-term trend and to determine if this pattern holds over an extended period or in different locations.

The study identified specific hotspots with consistently higher LST values, and a visual connection between LST and LULC changes was found in these areas. This suggests that land use changes, such as urban expansion, construction works, and other human activities, can visibly impact local LST. Understanding the connection between LST and LULC changes in these hotspots can help identify areas prone to urban heat islands effect and implement targeted mitigation strategies.

The study found a strong positive correlation between built-up areas and LST, similar to Weng (2001), indicating that urbanisation and the expansion of built-up areas could contribute to higher LST values. On the other hand, between LST, water, and vegetation, a strong negative correlation was observed. This suggests that the presence of water bodies can help moderate local LST. The negative correlation between LST and water is also in line with previous studies, as water bodies tend to have lower LST

due to their high heat capacity and evaporative cooling (Nichol, 1996; Xu, 2006). The negative correlation between LST and vegetation can be attributed to the cooling effect of vegetation through shade and evapotranspiration (Bonan, 2015; Zomer et al., 2008). The analysis revealed the presence of outlier values in both mean and maximum LST. This pattern suggests a recurring temperature anomaly every six or seven years, predominantly in the dry season. However, it is crucial to examine further using a broader dataset to substantiate these patterns and come to a definite conclusion about this more robustly.

The implications of these findings can be helpful for urban planning and management in the city and surrounding areas. Understanding the seasonal variability, LST trends, and the influence of land use changes on local LST values can help inform targeted strategies to mitigate the impacts of urban heat islands and promote sustainable urban development. For example, incorporating green and blue infrastructure in urban planning could help moderate local LST values and improve the overall urban environment.

The studies on time series of LST often produce a visible trend (Peng et al., 2012). There is an absence of a clear long-term trend in LST in this study's findings, despite the seasonal fluctuations and noticeable spikes in temperature. This outcome suggests that the LST dynamics in this area are complex and potentially influenced by various factors, including seasonal variability and human-induced land use changes.

4.4 Theoretical and practical implications of the study findings

The study supports the widely accepted theory that urbanisation and LULC changes are closely related to LST variations (Oke, 1982; Weng, 2001). The study highlights the importance of considering local context and specific LULC changes when examining LST dynamics. The study emphasises that a common approach to LST analysis may not be appropriate. A more nuanced and context-dependent understanding of LST dynamics is needed. This could involve incorporating local LULC changes and seasonal variability into existing theories and models and developing new frameworks that account for the complex interplay between LST and LULC changes in different settings. The study thus contributes to developing more refined and context-specific theoretical perspectives on LST dynamics, which can ultimately lead to improved urban planning and management strategies.

The study highlights the importance of considering local context and specific LULC changes when formulating urban planning and development policies. Decision-makers

can use these findings to develop more context-sensitive strategies that minimise the adverse effects of urbanisation on LST, such as promoting green spaces, preserving wetlands, and implementing sustainable building practices. Additionally, the research's technical framework can be used for monitoring LST. The technical framework of the study may inspire the development of new techniques that can help monitor and mitigate LST changes more effectively. For instance, advancements in remote sensing and GIS technologies could enable more precise tracking of LULC changes and LST dynamics at local and regional scales.

4.5 Limitations of the study

The results of this study are based on a specific study area, and the findings may not be universally applicable. However, the methodology employed in this study can be applied to other areas. Here is a list of some limitations of the study:

- The study area is prone to be affected by lots of clouds. This made finding images from precisely the same day each year difficult. In theory, that would help to compare LST in different timestamps more precisely. Hence, such a yearly comparison of LST might have introduced some inconsistency in absolute temperature measurement due to variations in image acquisition dates.
- While the study looked into changes in LST values in different timestamps considering changes in LULC, it did not consider other factors (e.g. local climate and climate-related anomalies) that can influence the LST besides the changes in LULC. Hence, it cannot be said that the changes in LST happened only because of LULC changes.
- Analysis of this study partially relied on a visual interpretation of LST and LULC changes, which may not provide precise information about the relationship between these variables. Future research could employ more advanced statistical or machine learning techniques to quantify this relationship and further examine the potential factors driving LST dynamics in the study area.
- The lack of a long-term trend in LST might be due to the limited time frame of the analysis. Extending the study period or comparing different locations might provide more insights into the factors influencing LST trends and patterns.
- Even though a strong correlation was found between LST and basic LULC classes, correlation always does not explain causation.

4.6 Future research directions

Based on the current study, several future research directions could further enhance the investigation of thermal dynamics and understanding of the relationships between LST and LULC changes.

While the spectral indices-based approach provides a means to compare LST and different indices values quantitatively, a detailed LULC would greatly help to interpret the relationship even more profoundly. However, it requires specific resources and efforts to get accurate high-resolution data. In this connection, thermal UAVs can be a valuable instrument for getting high-resolution thermal data on a small scale. Since UAVs are well suited for small areas, they can collect data on the hotspots identified from the satellite image analysis and look deeper to understand the relationship between LST and LULC and might provide a causal explanation.

The study provides valuable insights into the LST-LULC relationship in a specific urban context. Future research could focus on conducting similar longitudinal studies across various urban environments, including those with different climate conditions, population densities, and urbanisation patterns. By comparing the findings from these diverse contexts, researchers might identify common patterns, trends, and context-specific factors that influence the LST-LULC relationship.

Another future research direction can be evaluating the effectiveness of various urban planning strategies in different contexts. Quantifying the impacts of specific interventions, such as green spaces, green roofs, and sustainable building practices, can help inform policymakers and urban planners in developing more effective strategies to reduce UHI effects.

Climate change is expected to considerably affect LST and LULC patterns (IPCC, 2014). Future research could explore the combined effects of climate change and LULC changes on LST dynamics, providing a more comprehensive understanding of the factors that drive LST changes in urban areas. This would require developing and applying new models and analytical techniques for the complex interplay between climate change, LULC changes, and LST.

Future research could incorporate social and economic factors into the analysis, such as income levels, land ownership patterns, and public policies, to obtain a more holistic understanding of the LST-LULC relationship. This could help elucidate the drivers of LULC changes and their impacts on LST and identify potential barriers to implementing effective urban planning strategies.

5 Conclusion

In conclusion, this study has provided valuable insights into the spatiotemporal patterns of LST in the study area and the relationship between LST and LULC changes using remote sensing techniques. The research has shown the significance of considering seasonal variability, LST trends, and the response of LST to different LULC types in specific hotspots. By comparing the findings with previous research, the study has contributed to a deeper understanding of the relationship between LST and LULC changes and their implications for urban planning and management.

The results of this study emphasized adopting a subtle and context-dependent approach to LST analysis, which can ultimately lead to more effective urban planning and management strategies. The study's implications demonstrate the potential for developing new theories, frameworks, or models that account for the complex interplay between LST and LULC changes in different settings.

Despite the study's limitations, the methodology employed can be applied to other areas and serve as a foundation for future research. Several future research directions have been suggested, including conducting longitudinal studies across various urban environments, evaluating the effectiveness of urban planning strategies, exploring climate change and LULC changes together on LST dynamics, and incorporating social and economic factors into the analysis.

In closing, this study has contributed to understanding LST dynamics and the relationship between LST and LULC changes. The findings and recommendations provided in this research have the potential to inform urban planners, policymakers, and researchers as they work towards creating more sustainable and resilient urban environments.

References

- Amiri, R., Weng, Q., Alimohammadi, A., & Alavipanah, S. K. (2009). Spatial-temporal dynamics of land surface temperature in relation to fractional vegetation cover and land use/cover in the Tabriz urban area, Iran. *Remote sensing of environment*, 113(12), 2606-2617.
- Akbari, H., Pomerantz, M., & Taha, H. (2001). Cool surfaces and shade trees to reduce energy use and improve air quality in urban areas. *Solar energy*, 70(3), 295-310.
- Aniello, C., Morgan, K., Busbey, A., & Newland, L. (1995). Mapping micro-urban heat islands using Landsat TM and a GIS. *Computers & Geosciences*, 21(8), 965-969.
- Arnfield, A. J. (2003). Two decades of urban climate research: a review of turbulence, exchanges of energy and water, and the urban heat island. *International Journal of Climatology: a Journal of the Royal Meteorological Society*, 23(1), 1-26.
- Asimakopoulos, D. N. (2001). *Energy and climate in the urban built environment*. Earthscan.
- Bonan, G. B. (2015). *Ecological climatology: Concepts and applications*. New York, NY, USA: Cambridge University Press.
- Bouhennache, R., Bouden, T., Taleb-Ahmed, A., & Cheddad, A. (2019). A new spectral index for the extraction of built-up land features from Landsat 8 satellite imagery. *Geocarto International*, 34(14), 1531-1551.
- Box, G. E., Jenkins, G. M., Reinsel, G. C., & Ljung, G. M. (2015). *Time series analysis: forecasting and control*. John Wiley & Sons.
- Burden, R. L., Faires, J. D., & Burden, A. M. (2015). *Numerical analysis*. Cengage learning, 114.
- Carlson, Toby N.; Gillies, Robert R.; Perry, Eileen M. (1994). A method to make use of thermal infrared temperature and NDVI measurements to infer surface soil water content and fractional vegetation cover. In *Remote Sensing Reviews* 9 (1-2), pp. 161–173.
- Carlson, T. N., & Ripley, D. A. (1997). On the relation between NDVI, fractional vegetation cover, and leaf area index. *Remote sensing of Environment*, 62(3), 241-252.

Chander, G., & Markham, B. (2003). Revised Landsat-5 TM radiometric calibration procedures and postcalibration dynamic ranges. *IEEE Transactions on geoscience and remote sensing*, 41(11), 2674-2677.

Chander, G., Markham, B. L., & Helder, D. L. (2009). Summary of current radiometric calibration coefficients for Landsat MSS, TM, ETM+, and EO-1 ALI sensors. *Remote sensing of environment*, 113(5), 893-903.

City of Phnom Penh. (2020). Chbar Ampov District.
<https://www.phnompenh.gov.kh/en/our-city/chbar-ampov/> (last accessed on 25 May 2023)

Coppo, P., Mastrandrea, C., Stagi, M., Calamai, L., Barilli, M., & Nieke, J. (2013). The sea and land surface temperature radiometer (SLSTR) detection assembly design and performance. In *Sensors, Systems, and Next-Generation Satellites XVII* (Vol. 8889, pp. 256-279). SPIE.

Crist, E. P., & Cicone, R. C. (1984). A physically-based transformation of Thematic Mapper data---The TM Tasseled Cap. *IEEE Transactions on Geoscience and Remote sensing*, (3), 256-263.

Du, C., Ren, H., Qin, Q., Meng, J., & Zhao, S. (2015). A practical split-window algorithm for estimating land surface temperature from Landsat 8 data. *Remote sensing*, 7(1), 647-665.

Dutta, D., Rahman, A., & Kundu, A. (2015). Growth of Dehradun city: An application of linear spectral unmixing (LSU) technique using multi-temporal landsat satellite data sets. *Remote Sensing Applications: Society and Environment*, 1, 98-111.

Erell, E., Pearlmutter, D., & Williamson, T. (2012). *Urban microclimate: designing the spaces between buildings*. Routledge.

Foga, S., Scaramuzza, P. L., Guo, S., Zhu, Z., Dilley Jr, R. D., Beckmann, T., ... & Laue, B. (2017). Cloud detection algorithm comparison and validation for operational Landsat data products. *Remote sensing of environment*, 194, 379-390.

Flynn, L. P., Harris, A. J., & Wright, R. (2001). Improved identification of volcanic features using Landsat 7 ETM+. *Remote Sensing of Environment*, 78(1-2), 180-193.

Gillies, R. R.; Kustas, W. P.; Humes, K. S. (1997): A verification of the 'triangle' method for obtaining surface soil water content and energy fluxes from remote measurements of the Normalized Difference Vegetation Index (NDVI) and surface e . In *International Journal of Remote Sensing* 18 (15), pp. 3145–3166.

Grimm, N. B., Faeth, S. H., Golubiewski, N. E., Redman, C. L., Wu, J., Bai, X., & Briggs, J. M. (2008). Global change and the ecology of cities. *science*, 319(5864), 756-760.

Hajat, S., O'Connor, M., & Kosatsky, T. (2010). Health effects of hot weather: from awareness of risk factors to effective health protection. *The Lancet*, 375(9717), 856-863.

He, C., Shi, P., Xie, D., & Zhao, Y. (2010). Improving the normalized difference built-up index to map urban built-up areas using a semiautomatic segmentation approach. *Remote Sensing Letters*, 1(4), 213-221.

Hondula, D. M., Georgescu, M., & Balling Jr, R. C. (2014). Challenges associated with projecting urbanization-induced heat-related mortality. *Science of the total environment*, 490, 538-544.

IPCC. (2014). Climate Change 2014: Synthesis Report. Contribution of Working Groups I, II and III to the Fifth Assessment Report of the Intergovernmental Panel on Climate Change. *IPCC*.

Jacob, D. J., & Winner, D. A. (2009). Effect of climate change on air quality. *Atmospheric environment*, 43(1), 51-63.

Jiménez-Muñoz, J. C., & Sobrino, J. A. (2003). A generalized single-channel method for retrieving land surface temperature from remote sensing data. *Journal of geophysical research: atmospheres*, 108(D22).

Jiménez-Muñoz, J. C., Cristóbal, J., Sobrino, J. A., Sòria, G., Ninyerola, M., & Pons, X. (2008). Revision of the single-channel algorithm for land surface temperature retrieval from Landsat thermal-infrared data. *IEEE Transactions on geoscience and remote sensing*, 47(1), 339-349.

Jiménez-Muñoz, J. C., Sobrino, J. A., Skoković, D., Mattar, C., & Cristobal, J. (2014). Land surface temperature retrieval methods from Landsat-8 thermal infrared sensor data. *IEEE Geoscience and remote sensing letters*, 11(10), 1840-1843.

Kleerekoper, L., Van Esch, M., & Salcedo, T. B. (2012). How to make a city climate-proof, addressing the urban heat island effect. *Resources, Conservation and Recycling*, 64, 30-38.

Kovats, R. S., & Hajat, S. (2008). Heat stress and public health: a critical review. *Annu. Rev. Public Health*, 29, 41-55.

Kumar, A., Pandey, A. C., & Jeyaseelan, A. T. (2012). Built-up and vegetation extraction and density mapping using WorldView-II. *Geocarto international*, 27(7), 557-568.

Lantz, T. C., Gergel, S. E., & Henry, G. H. (2010). Response of green alder (*Alnus viridis* subsp. *fruticosa*) patch dynamics and plant community composition to fire and regional temperature in north-western Canada. *Journal of Biogeography*, 37(8), 1597-1610.

Li, Z. L., Tang, B. H., Wu, H., Ren, H., Yan, G., Wan, Z., ... & Sobrino, J. A. (2013). Satellite-derived land surface temperature: Current status and perspectives. *Remote sensing of environment*, 131, 14-37.

Li, X., Zhou, Y., Zhu, Z., Liang, L., Yu, B., & Cao, W. (2018). Mapping annual urban dynamics (1985–2015) using time series of Landsat data. *Remote Sensing of Environment*, 216, 674-683.

Maktav, D., & Erbek, F. S. (2005). Analysis of urban growth using multi-temporal satellite data in Istanbul, Turkey. *International Journal of Remote Sensing*, 26(4), 797-810.

McFeeters, S. K. (1996). The use of the Normalized Difference Water Index (NDWI) in the delineation of open water features. *International journal of remote sensing*, 17(7), 1425-1432.

Meehl, G. A., & Tebaldi, C. (2004). More intense, more frequent, and longer lasting heat waves in the 21st century. *Science*, 305(5686), 994-997.

Mekong River Commission. (2021). Mekong flood forecasting.
<http://www.mrcmekong.org/> (*last accessed on 24 May 2023*).

Meteorological Department of Cambodia. (2021). Climate data of Cambodia.
<http://www.cammet.gov.kh/> (*last accessed on 25 May 2023*).

Mildrexler, D. J., Zhao, M., & Running, S. W. (2011). A global comparison between station air temperatures and MODIS land surface temperatures reveals the cooling role of forests. *Journal of Geophysical Research: Biogeosciences*, 116(G3).

Mohamed, A., & Worku, H. (2019). Quantification of the land use/land cover dynamics and the degree of urban growth goodness for sustainable urban land use planning in Addis Ababa and the surrounding Oromia special zone. *Journal of Urban Management*, 8(1), 145-158.

Moran, M. S., Vidal, A., Troufleau, D., Qi, J., Clarke, T. R., Pinter Jr, P. J., ... & Neale, C. M. U. (1997). Combining multifrequency microwave and optical data for crop management. *Remote Sensing of Environment*, 61(1), 96-109.

Montanaro, M., Barsi, J., Lunsford, A., Rohrbach, S., & Markham, B. (2014). Performance of the Thermal Infrared Sensor on-board Landsat 8 over the first year on-orbit. In *Earth Observing Systems XIX* (Vol. 9218, pp. 375-388). SPIE.

Nagler, P. L., Glenn, E. P., Nguyen, U., Scott, R. L., & Doody, T. (2013). Estimating riparian and agricultural actual evapotranspiration by reference evapotranspiration and MODIS enhanced vegetation index. *Remote Sensing*, 5(8), 3849-3871.

National Institute of Statistics. (2020). Population statistics of Cambodia.
<http://www.nis.gov.kh/> (*last accessed on 25 May 2023*).

Nguyen, L. H., Nghiem, S. V., & Henebry, G. M. (2018). Expansion of major urban areas in the US Great Plains from 2000 to 2009 using satellite scatterometer data. *Remote Sensing of Environment*, 204, 524-533.

Nichol, J. E. (1996). High-resolution surface temperature patterns related to urban morphology in a tropical city: A satellite-based study. *Journal of Applied Meteorology and Climatology*, 35(1), 135-146.

Nichol, J. E., Fung, W. Y., Lam, K. S., & Wong, M. S. (2009). Urban heat island diagnosis using ASTER satellite images and 'in situ' air temperature. *Atmospheric Research*, 94(2), 276-284.

Nill, L., Ullmann, T., Kneisel, C., Sobiech-Wolf, J., & Baumhauer, R. (2019). Assessing spatiotemporal variations of Landsat land surface temperature and multispectral indices in the Arctic Mackenzie Delta Region between 1985 and 2018. *Remote Sensing*, 11(19), 2329.

Nitze, I., & Grosse, G. (2016). Detection of landscape dynamics in the Arctic Lena Delta with temporally dense Landsat time-series stacks. *Remote Sensing of Environment*, 181, 27-41.

Oke, T. R. (1982). The energetic basis of the urban heat island. *Quarterly journal of the royal meteorological society*, 108(455), 1-24.

Oke, T. R., & Cleugh, H. A. (1987). Urban heat storage derived as energy balance residuals. *Boundary-Layer Meteorology*, 39, 233-245.

Patz, J. A., Campbell-Lendrum, D., Holloway, T., & Foley, J. A. (2005). Impact of regional climate change on human health. *Nature*, 438(7066), 310-317.

Pearson, K. (1920). Notes on the history of correlation. *Biometrika*, 13(1), 25-45.

Peng, S., Piao, S., Ciais, P., Friedlingstein, P., Ottle, C., Bréon, F. M., ... & Myneni, R. B. (2012). Surface urban heat island across 419 global big cities. *Environmental science & technology*, 46(2), 696-703.

Pickett, S. T., Cadenasso, M. L., & Grove, J. M. (2004). Resilient cities: meaning, models, and metaphor for integrating the ecological, socio-economic, and planning realms. *Landscape and urban planning*, 69(4), 369-384.

Rahman, A., Kumar, S., Fazal, S., & Siddiqui, M. A. (2012). Assessment of land use/land cover change in the North-West District of Delhi using remote sensing and GIS techniques. *Journal of the Indian Society of Remote Sensing*, 40, 689-697.

Rouse Jr, J. W., Haas, R. H., Schell, J. A., & Deering, D. W. (1973). *Monitoring the vernal advancement and retrogradation (green wave effect) of natural vegetation* (No. NASA-CR-132982).

Saaroni, H., Ben-Dor, E., Bitan, A., & Potchter, O. (2000). Spatial distribution and microscale characteristics of the urban heat island in Tel-Aviv, Israel. *Landscape and urban planning*, 48(1-2), 1-18.

Sandholt, I., Rasmussen, K. and Andersen, J., (2002). A simple interpretation of the surface temperature/vegetation index space for assessment of surface moisture status. *Remote Sensing of Environment*, 79(2-3), pp.213-224.

Santamouris, M. (2014)a. On the energy impact of urban heat island and global warming on buildings. *Energy and Buildings*, 82, 100-113.

Santamouris, M. (2014)b. Cooling the cities—a review of reflective and green roof mitigation technologies to fight heat island and improve comfort in urban environments. *Solar energy*, 103, 682-703.

Scaramuzza, P., Micijevic, E., & Chander, G. (2004). SLC gap-filled products phase one methodology. *Landsat Technical Notes*, 5.

Sobrino, J. A., Raissouni, N., & Li, Z. L. (2001). A comparative study of land surface emissivity retrieval from NOAA data. *Remote Sensing of Environment*, 75(2), 256-266.

Sobrino, J. A., Jiménez-Muñoz, J. C., Sòria, G., Romaguera, M., Guanter, L., Moreno, J., ... & Martínez, P. (2008). Land surface emissivity retrieval from different VNIR and TIR sensors. *IEEE transactions on geoscience and remote sensing*, 46(2), 316-327.

Storey, J., Scaramuzza, P., & Barsi, J. (2005). Landsat 7 scan line corrector-off gap-filled product development. In *Proceeding of Pecora* (Vol. 16, pp. 23-27).

Wan, Z. (2008). New refinements and validation of the MODIS land-surface temperature/emissivity products. *Remote sensing of Environment*, 112(1), 59-74.

Wan, Z., Zhang, Y., Zhang, Q., & Li, Z. L. (2004). Quality assessment and validation of the MODIS global land surface temperature. *International journal of remote sensing*, 25(1), 261-274.

Weng, Q. (2001). A remote sensing? GIS evaluation of urban expansion and its impact on surface temperature in the Zhujiang Delta, China. *International journal of remote sensing*, 22(10), 1999-2014.

Weng, Q. (2009). Thermal infrared remote sensing for urban climate and environmental studies: Methods, applications, and trends. *ISPRS Journal of photogrammetry and remote sensing*, 64(4), 335-344.

Weng, Q., Lu, D., & Schubring, J. (2004). Estimation of land surface temperature–vegetation abundance relationship for urban heat island studies. *Remote sensing of Environment*, 89(4), 467-483.

Weng, Q., Liu, H., Liang, B., & Lu, D. (2008). The spatial variations of urban land surface temperatures: pertinent factors, zoning effect, and seasonal variability. *IEEE Journal of Selected Topics in Applied Earth Observations and Remote Sensing*, 1(2), 154-166.

Xu, H. (2006). Modification of normalised difference water index (NDWI) to enhance open water features in remotely sensed imagery. *International journal of remote sensing*, 27(14), 3025-3033.

Xu, H. (2008). A new index for delineating built-up land features in satellite imagery. *International journal of remote sensing*, 29(14), 4269-4276.

Zha, Y., Gao, J., & Ni, S. (2003). Use of normalized difference built-up index in automatically mapping urban areas from TM imagery. *International journal of remote sensing*, 24(3), 583-594.

Zhang, P., Imhoff, M. L., Wolfe, R. E., & Bounoua, L. (2010). Characterizing urban heat islands of global settlements using MODIS and nighttime lights products. *Canadian Journal of Remote Sensing*, 36(3), 185-196.

Zhou, Y., Yang, G., Wang, S., Wang, L., Wang, F., & Liu, X. (2014). A new index for mapping built-up and bare land areas from Landsat-8 OLI data. *Remote Sensing Letters*, 5(10), 862-871.

Zomer, R. J., Trabucco, A., Bossio, D. A., & Verchot, L. V. (2008). Climate change mitigation: A spatial analysis of global land suitability for clean development mechanism afforestation and reforestation. *Agriculture, ecosystems & environment*, 126(1-2), 67-80.

Appendix

1. Table for sensor-wise number of images (related to section [2.1](#))

Sensor	Number of images
Landsat 5 (1984-2012)	115
Landsat 7 (1999-2021)	213
Landsat 8 (2013-Present)	134
Total	462

2. Table for seasonal variation from 2015 (related to section [3.2](#))

Month	Min LST	Mean LST	Max LST
January	25.3	28.46	38.15
February	26.66	32.91	45.02
April	31.36	39.73	54.49
May	26.94	34.37	47.31
June	28.83	37.14	49.54
September	20.1	24.67	33.6
October	29.83	34.11	46.41
December	23.48	26.67	34.13

3. Table for yearly comparison and warmth score (related to section [3.1](#))

Year	Minimum LST	Mean LST	Maximum LST	
	No. of months	No. of months	No. of months	
	MinLST ($\geq 28^{\circ}\text{C}$)	MeanLST ($\geq 32^{\circ}\text{C}$)	MaxLST ($\geq 42^{\circ}\text{C}$)	Warmth score
2000	3	5	5	13
2001	1	3	4	8
2002	3	5	6	14
2003	4	4	4	12
2004	2	7	8	17
2005	3	7	6	16
2006	5	7	9	21
2007	3	4	7	14
2008	2	4	5	11
2009	2	6	8	16
2010	3	4	6	13
2011	2	3	7	12
2012	0	2	4	6
2013	2	2	5	9
2014	1	2	4	7
2015	2	7	8	17
2016	2	4	8	14
2017	2	1	2	5
2018	1	3	4	8
2019	2	3	5	10

	Minimum LST	Mean LST	Maximum LST	
	No. of months	No. of months	No. of months	
Year	MinLST ($\geq 28^{\circ}\text{C}$)	MeanLST ($\geq 32^{\circ}\text{C}$)	MaxLST ($\geq 42^{\circ}\text{C}$)	Warmth score
2020	0	5	6	11
2021	2	4	3	9

4. Yearly temperature range (related to [3.1](#))

Year	MinLST	MaxLST
2000	23.620267	39.246831
2001	24.143079	39.542192
2002	24.528403	44.077427
2003	27.837822	43.799108
2004	25.401349	43.703277
2005	25.869049	43.833724
2006	27.250059	47.931487
2007	24.570124	45.229699
2008	23.849363	41.987479
2009	25.894126	47.446718
2010	25.848326	45.921738
2011	24.029453	44.043398
2012	21.861331	42.949105
2013	22.221769	41.682483
2014	22.422889	41.205478
2015	25.665606	45.406316
2016	24.732166	45.97173
2017	22.068277	39.389134
2018	22.995234	40.801275
2019	24.071847	43.334138
2020	23.021131	41.629851
2021	24.237837	41.264895

5. Data tables extracted from LST and for Correlation test

The data tables extracted from LST and for correlation test can be found at:

https://github.com/mohigeo33/lst_timeseries/blob/main/CSV%20files.zip

6. Shapefile for the study area

Shapefile for the study area can be found at:

https://github.com/mohigeo33/lst_timeseries/blob/main/AOI.zip

7. Shapefile for the study area

The codes used for LST estimation and statistical analysis can be found at:

https://github.com/mohigeo33/lst_timeseries